Monte-Carlo simulation of lepton pair production in "$\bar{p}p \to l^+l^- + X$" events at $E_{beam} = 14$ GeV.

A.N. Skachkova, N.B. Skachkov,
Joint Institute for Nuclear Research, Dubna, 141980, Russia
E-mail:Anna.Skachkova@cern.ch, skachkov@jinr.ru

February 2, 2008

Abstract

The process of lepton pair production in antiproton-proton collisions at PANDA experiment is simulated for studying the distributions of energy, transverse momentum and angle variables of individual leptons created in a antiquark-quark annihilation subprocess $q\bar{q} \to l^+l^-$. The correlations between mentioned above physical variables and the corresponding distributions of the number of events versus the values of these variables are presented.

A special attention is paid to the distributions that describe the produced l^+l^--system as a whole system. It is shown that the spectrum of the total energy of l^+l^- pair may spread from 1 GeV up to 12 GeV and in about a half of events its energy is higher than 5 GeV, i.e. the produced pairs are rather energetic. It is argued that the measurement of the total transverse momentum of a lepton pair as a whole may provide an important information about an intrinsic transverse momentum $< k_T >$ that appear due to the Fermi motion of quarks inside the nucleon.

The problems due to the presence of fake leptons that appear from meson decays are discussed also. It is shown that in muon pair production case about of 40% of events may not contain charged pions at all in their final state, i.e. they would be free of fake muons. In the remaining part of events, the information about the muon production vertex and the moderate PT^{μ}-cuts from below may be also useful for discrimination of fake muons. The contribution from the background processes that may contain leptons is discussed also.

1 Introduction.

Quark-antiquark annihilation subprocess of the hadron-hadron collision, mentioned in the abstract (see [1] and [2]), may provide an interesting information about the quark dynamics inside the hadron. The results of measuring of lepton pairs, produced in these

collisions at high energies [3], were already used to enlarge our knowledge about the structure functions that describe the parton distributions in hadrons [4].

Due to a limited size of a range of avaliable total energy PANDA would be rather an intermediate than a high energy experiment. In this energy region the important role plays the physics of bound states and resonances, which is strongly connected with the quark confinement problem.

At the same time it is well known from the previous $p\bar{p}$ experiments, done at low energies (like the $p\bar{p}$ annihilation experiments done at LEAR at CERN), that many features of the resonance decays may be also quite well explained, basing on the simple phenomenological rules, like the so called quark line rule [5].

Recently, the OBELIX Collaboration (CERN) has published the results of a detailed analysis of three reactions of the annihilation at rest with the three mesons production in the final state: $p\bar{p} \to \pi^+\pi^-\pi^0, K^+K^-\pi^0, \pi^\pm\pi^\mp K^0$ [6], [7]. The analysis done in these articles also does not exclude the possibility that some features of the observed resonant structures, or enhancements, as well as the observation of some resonant structures suppression in the S- and P-waves of the $p\bar{p}$ system, which undergo the annihilation process at rest, may need the SU_3 model application for their explanation.

From here we may conclude that if we shall consider a case of the antiproton scattering off the proton target in a case of the antiproton beam of 14 GeV energy [1] (that corresponds to the center of mass energy of the $p\bar{p}$ system $E_{cm} = 5.3GeV$), then it would be quite natural to use a quark parton model to describe the $\bar{p}p \to l^+l^- + X$ process. To this reason [2] we have used here the PYTHIA event generator [9], which is based on the ideas of the quark parton model and is well tested and widely used for the simulation of high energy hadron-hadron interactions. Some parameters of the generator were set here, following [8], to those values that allow fast and reliable simulation in the case of E_{beam}=14 GeV.

It is important to note that PYTHIA simulation is based on the use of the amplitudes of the relativistic quantum field theory. In our case it is the perturbative QCD amplitude of the $q\bar{q} \to l^+l^-$ subprocess, implemented into the PYTHIA package. This allows a proper account of the relativistic kinematics while simulation of the distributions of different physical variables, connected with the $\mu^+\mu^-$- (or e^+e^--) pairs produced in event.

It is worth to mention also that in any case the dominant mechanism of the lepton-anti-lepton pair production would be one and the same in the most of another than perturbative QCD approaches or models. Really, in this special case of $p\bar{p} \to l\bar{l} + X$ process the dominant contribution to the process amplitude in any model would come from one and the same amplitude of quark pair annihilation $q\bar{q} \to l\bar{l}$ in the chosen range of beam energy value.

It should be mentioned that PYTHIA generates the events in which the final state particles are produced in a result of a rather long chain of interactions. This chain includes the primary partons, which are produced in a hard perturbative $2 \to 2$ quark-parton fundamental subprocess and latter on do pass the stage of interaction between themselves (which is described by the LUND string fragmentation model [16] - [21] used

[1] this value of energy was used also in our previous Note [8], devoted to muon pair production study.

[2] other arguments may be found in [8].

in PYTHIA). After this the quarks, diquarks and strings, produced at this stage, do pass the hadronization phase. The variety of the produced elementary particles then undergo a stage of decays in a case of the presence of the nonstable particles or resonances among them. At the end of the simulation there are left only free particles in the final state. Therefore, while using the PYTHIA, we may get, as the result of simulation, only the distributions of free particles, unbiased by any detector effects like, for example, by a magnetic field. The account of the influence of the detector effects would be a subject of the following papers.

In the Section 2, devoted to lepton distributions, the results of the previous Note [8] will be added by a number of new 3- and 2-dimensional plots that show different kind of correlations (like Energy-Energy and Angle-Angle correlations) between the physical variables of the leptons, produced in the quark level subprocess $q\bar{q} \to l^+l^-$. All plots of this Note are collected in the Appendix (Section 7:"Figures").

Let us mention that the main results of this Note (Sections 2, 3 and 4) are valid for a case of muon pair as well as for the electron-positron pair production. To this reason in these three Sections we shall speak about the distributions obtained for the lepton case because muon distributions are practically do not differ from the electron ones (so, the word "muon" is equal to the "electron " in the Sections 2,3 and 4). The main difference of e^+e^- case from that one of $\mu^+\mu^-$ pair production would appear only while considering the "background" contribution from the fake muons (see Sections 5 and 6).

The next important new addition, as comparing to [8], is presented in the Section 3, where the distributions of some global variables, that describe the produced muon or electron pair as a whole system, like for instance, the invariant mass of the signal lepton pair. Among them of most interest is the total transverse momentum of a lepton pair, which value is connected with the intrinsic transverse velocity of a quark inside the proton. Recent results of the experiment E706 on the direct photon production, performed at Fermilab [11], have shown that the averaged value of the quark transverse momentum in the proton may be of $< k_T > \approx 1.4$ GeV order. Two sources of a possible appearance of quark transverse momentum in the proton, i.e. the intrinsic Fermi motion of quark inside the proton and the influence of an initial state radiation, are studied in Section 3. It is pointed out that due to the fact that the transverse motion of quark in the nucleon does not depend on the value of the boost along the beam line, there is a unique possibility for PANDA to measure the value of quark $< k_T >$, which is so important for a precise setting of the absolute scale of jet energy [12] - [14] and thus for a precise determination of particles mass (like of top quark and may be of Higgs boson and SUSY particles) in the experimental measurements at Tevatron and LHC.

Let us noted that each generator has its own internal restrictions. In present generation we had, due to the internal PYTHIA cuts, a restriction on the value of the invariant mass, produced in a fundamental $2 \to 2$ hard QCD subprocess. In practice, the value of the invariant mass of a muon (electron) pair, produced in a signal event, turned out to be restricted by the limit from below: $M_{inv}^{l^+l^-} > 1$ GeV. The influence of this cut on the spectrum of the signal lepton pair energy will be discussed in the Sections 3 and 4.

The problem of fake muons background is discussed in the last Section 5. We do not

consider here a case of a contribution from the events, defined by another than $q\bar{q} \to \mu^+\mu^-$ subprocess, because, as far as we have an aim to study the muon pair production (i.e., a case of muon pair which has a common vertex) the appearance of this pair from some vector mesons decays would not be so large. Nevertheless we plan to study it in the nearest future. The main problem is caused by the presence of the fake muons from pions decays in the same $p\bar{p}$ process (based on the annihilation $q\bar{q} \to \mu^+\mu^-$ subprocess). [3]

As the first step the number of events that would not contain at all the charged pions in the final state is estimated in Section 5. The simulation has shown that the fraction of such events without fake decay muons may turn out to be not a small one. The distribution of the number of fake muons versus their PT value, presented in Section 5, provides an information for the proper choice of an effective additional cut for their discrimination. Section 5 includes also the distributions of x-,y- and z-components of the position of the vertex of the fake muons production, which may be also useful for their separation. In Section 6 the spectra of background leptons, mainly electrons, produced in other than $q\bar{q} \to l^+l^-$ QCD subprocesses, are presented.

2 Muon/electron distributions in $p\bar{p}$ collisions.

We have done the generation of 100 000 [4] "$\bar{p}p \to l^+l^- + X$" events with $2 \to 2$ QED $q\bar{q} \to \gamma^* \to l^+l^-$ subprocess. In what follows these events should be called as "signal events", and, respectively, the muons (electrons) that are produced in hard QED $q\bar{q} \to l^+l^-$ subprocess would be called as the "signal" leptons. Those leptons that appear in events due to hadron (mainly mesons) decays will be called as "decay" leptons.

The distributions of the number of generated signal events versus the values of the energy $E^{l^{(+/-)}}$ of the signal leptons, as well as versus the modulus of the transverse momentum $PT^{l^{(+/-)}}$ [5] and of the polar angles $\theta^{l^{(+/-)}}$, measured from the beam direction (they are denoted in plots as $TETA^l$) are shown (from top to bottom, respectively) in the Figure 1 of the Section 7 (Appendix: "Figures"), which contains all plots and figures. The left hand column in the Figure 1 is for l^- distributions and the right one is for l^+. No difference is seen between l^+ and l^- distributions.

One can see from the top raw of Figure 1 that the energy of leptons may vary in the interval $0 < E^l < 10GeV$ with a mean value $< E^l >= 2.6$ GeV and its spectrum has a peak at a rather small value of about E^l_{peak} =0.4 GeV.

The PT^l spectrum (see the middle raw of Figure 1) has an analogous peak position at $PT^l_{peak} = 0.5$ GeV. Behind their peaks both E^l and PT^l spectra falls rather steeply but

[3] or from fake electrons in a case of $q\bar{q} \to e^+e^-$ process. It is clear that the appearance of this kind of fake electrons in the same signal annihilation $\bar{p}p \to e^+e^-$ process has a negligibly small probability as comparing with the case of fake muons from pion decays.

[4] this number allows an easy estimation of the number of events that shall pass any momentum or angle cuts by a help of the correlation plots which are obtained in ROOT "TEXT" format [10] and do contain the information in the numerical form.

[5] In all plots of Section 7 it is supposed that the energy and the PT scales are presented in GeV units (c=1 system is used) while for the angle scales the degrees measure is used.

the spectrum of PT^l is confined in a more narrow interval $0 < PT^l < 2$ GeV.

The number of events (N_{event}) spectrum versus the polar angle θ^l (see bottom raw) has a peak around $\theta^l = 10^o$ and the mean value $< \theta^l >= 28.4^o$. We see that while the most of signal leptons are scattered into the forward direction ($\theta^l < 90^o$) still there is a small number of them which may fly even into the backward hemisphere ($\theta^l > 90^o$).

It is useful to have the set of plots done separately for the signal leptons having the largest energy (we shall call them as "fast" leptons in what follows) in the lepton pair, produced in an event, and, correspondingly, for those, having a smaller energy ("slow" lepton in a pair). This set of plots for the signal leptons is given in Figure 2 of the Appendix, where the left hand column shows the distributions of "slow" leptons while the right one is for the "fast" leptons distribution.

One can see from Figure 2 that the energy spectrum of the fast signal leptons (top raw) grows up rather fast from the point $E^l_{fast} = 0.5GeV$ (more than 90% of fast leptons have $E^l_{fast} > 1GeV$) up to the peak position at the point $E^l_{fast} = 2.5GeV$ and then practically vanishes at $E^l_{fast} = 10GeV$.

In contrast to this picture the spectrum of the less energetic signal leptons (left raw) has a peak around the point E^l_{slow}=0.4 GeV (where the spectrum of fast leptons only starts) and then it vanishes at the point, which practically do corresponds to the mean value of the most energetic signal leptons, i.e. at $< E^l_{fast} > = 3.8$ GeV. One may see that the spectrum of slow leptons in a pair is a very different from that one of fast leptons.

The difference between the PT^l spectra (see the middle raw of Figure 2) of fast and slow leptons seams not to be so large. It results only in about of 340 MeV shift to the left of the peak position of slow leptons spectrum as well as in the corresponding end point shift to the left. Both of these spectra do demonstrate that the main part of slow as well as of fast leptons have $PT^l > 0.2$ GeV.

This similarity of PT^l spectra of fast and slow leptons results (due to a large difference of their energy spectra, i.e. of P^l_z components) in a large difference of their polar angle θ^l distributions (see bottom raw in Figure 2). Really, the θ^l_{slow} spectrum is shifted to the right to the higher values, as comparing to that one of θ^l_{fast}. Note also that their mean value $< \theta^l_{slow} > = 40^o$ is a more than two times higher than the analogous mean value of the fast leptons: $< \theta^l_{fast} >= 16^o$.

Another and the most important difference that is seen from these angular distributions is that all fast leptons fly in the forward direction ($\theta^l_{fast} < 90^o$) and their spectrum practically finishes at $\theta^l_{fast} = 60^o$, while about of 17% of slow leptons have $\theta^l_{slow} > 60^o$. It is worth to mention that about of 5% of slow leptons may scatter into the back hemisphere.

The number (or percentage) of signal leptons, scattered into the forward or back hemispheres, may be easily found from the 3-dimensional "Angle - Energy" correlation plots, presented in Figures 3,4 and 5 (see Section 7, Appendix) done by help of ROOT [10]). The left hand side of Figure 3 contains the "LEGO1" ROOT plot with the distribution of the number of generated events versus:

• the energy E^l_{slow} of the less energetic leptons in l^+l^- pair (the energy axis is on the right hand side of this plot and its scale is given in GeV units), as well as versus:

• the polar angles θ^l_{slow} (the angle axis is on the left hand side of a plot and the scale on it is given in a degree measure units).

The right hand column contains the analogous "Angle- Energy" correlation plots with the distributions of the number of events versus the energy E^l_{fast} of the most energetic leptons in a l^+l^- pair, as well as versus their polar angles θ^l_{fast}. These plots show the correlation between the angle and the energy of slow and fast leptons in a l^+l^- pair in event, as well as the distribution of the number of events for the correlated values of these variables. It becomes much more easy to see these numbers after making the projection of these surfaces onto a plane.

The projections of these 3-dimensional distributions onto the 2-dimensional θ/E - planes are shown in Figures 4 and 5. The correspondence between the color contours in Figure 4 (SURF2Z plots) and the number of events per unit of a bin square is defined by the vertical color scale, included into the right hand side of each plot. For a convenience of counting of the number of events in each bin square of the 2-dimensional θ^l/E^l planes we present in the Figure 5 the "TEXT" ROOT analogs of plots from Figure 4. The exact numbers in each square bin may be seen by a help of the zoom application to this place of .ps file plots. [6] From these plots one can see that the most of slow leptons that fly into the back hemisphere, i.e. $\theta^l_{slow} > 90^o$, (on total it is about about of 5.5% of events with l^+l^- pairs), do have the energy which is less than $E^l_{slow} = 0.5$ GeV.

The number of events distribution versus the energies of leptons in a pair (slow and fast leptons in a pair), i.e. that come from pions decays. the "Energy-Energy" correlation, as well as versus the angles of both leptons in a pair, i.e. the "Angle-Angle" correlation, are shown in the 3-dimensional "LEGO1" ROOT plots in Figure 6 of Section 7 (Appendix). The projections of these 3-dimensional plots onto the Energy-Energy E^l_{slow}/E^l_{fast} plane (left hand side), as well as onto the Angle-Angle $\theta^l_{slow}/\theta^l_{fast}$ plane (right hand side), are shown in Figure 7 (as for the ROOT "SURF2Z" color contour plots) and in Figure 8 (as for the ROOT "TEXT" numerical plots).

From Figures 7 and 8 we may conclude that among the signal events with l^+l^- pairs there are :

• about of 14% of them have lepton pairs with the polar angles belonging to the square, defined by the following bounds:

$$\theta^l_{slow}, \theta^l_{fast} < 20^o;$$

• about of 40% of events do have lepton pairs which angles are contained in a square:

$$\theta^l_{slow}, \theta^l_{fast} < 40^o \ .$$

[6] or use the central plate on PC mouse to click on the place you are interested with in the .ps file of the Section 7 (Appendix) and choose the zoom grade.

• about of 72% of events do have lepton pairs which angles fit into a more wide square:

$$\theta^l_{slow}, \theta^l_{fast} < 60^o.$$

• and there is about of 94% of events, which angles are restricted by the relations:

$$\theta^l_{slow}, \theta^l_{fast} < 90^o.$$

It means that in case, when the lepton system would cover the angle region $\theta^l \leq 90^o$, then less than 6% of events, which do contain the l^+l^- signal pairs, would be lost.

From the Figure 2 and the Energy-Energy correlation plots shown in the Figures 7 and 8 one may see that:

• if the following loose cut from below would be applied to the energy of both (fast and slow) leptons in a pair (recall about the peak at $E^l_{slow} = 0.4GeV$)

$$E^l_{fast}, E^l_{slow} > 0.5GeV \ ,$$

then more than 25% of simulated signal events with lepton pairs would be lost,

• but in a case of setting of a more strict cut:

$$E^l_{fast}, E^l_{slow} > 1GeV \ ,$$

then about of 45% of simulated events with signal lepton pairs would be lost.

3 Global variables for $q\bar{q} \to \gamma^* \to l^+l^-$ subprocess. u- and d- quarks components of a proton structure function .

So far we considered the distributions of physical variables that describe the individual features of leptons belonging to a l^+l^- pair. Here we shall discuss a set of variables which characterize the lepton pair system (and the quark-antiquark system) as a whole.

Figure 9 of Section 7 (Appendix) contains the plots that present the distributions of the number of generated events versus the most typical physical variables that may describe the initial and final states of two particle systems which appear in the annihilation subprocess $q\bar{q} \to \gamma^* \to l^+l^-$. Let us firstly mention those of them which include different components of the total 4-momentum P^{l+l-}_α $(\alpha = 0, 1, 2, 3)$ of a lepton pair :

$$P^{l+l-}_\alpha = P^{l^+}_\alpha + P^{l^-}_\alpha . \tag{1}$$

The distribution of the total energy of a lepton system

$$E^{l^+l^-} = E^{l^+} + E^{l^-}, \tag{2}$$

is shown in the right hand plot of the middle raw of Figure 9 of Appendix (and noted there as the "E-l+l- distribution"). The longitudinal component distribution

$$P_z^{l^+l^-} = P_z^{l^+} + P_z^{l^-} \tag{3}$$

(noted there as "Pz-l+l- distribution") is included into the left hand side plot of the same middle raw. These two plots look very similar. The explanation of this fact follows from the form of the plot for the transversal component

$$\vec{P}_T^{l^+l^-} = \vec{P}_T^{l^+} + \vec{P}_T^{l^-}, \tag{4}$$

namely, of its modulus

$$P_T^{l^+l^-} = |\vec{P}_T^{l^+l^-}| = |\vec{P}_T^{l^+} + \vec{P}_T^{l^-}|, \tag{5}$$

which is presented as "$PT - l + l - distribution''(\equiv P_T^{l^+l^-})$ in the left bottom corner of Figure 9. From here one may see that the transversal component distribution is, really, much more narrower (its mean value is about 1 GeV) than those of $P_z^{l^+l^-}$ and $E^{l^+l^-}$ distributions. Thus, the main contribution to the value of the lepton pair energy comes from the longitudinal component $P_z^{l^+l^-}$. It is worth to mention that both of $P_z^{l^+l^-}$ and $E^{l^+l^-}$ distributions do not start exactly from the zero values. The starting point of the total energy $E^{l^+l^-}$ spectrum is around 1 GeV. [7] It is important to mention that the spectrum of a lepton pair energy in $\bar{p}p$ collision has the mean value around 5 GeV (as well as the spectrum of the $P_z^{l^+l^-}$ component).

It means that on average the lepton pair caries a bit more than 1/3 of the total energy (in the rest frame of the proton) of the $\bar{p}p$-system. From the same right hand plot of the middle raw of Figure 9 it is clearly seen that in about a half of events the energy of a lepton pair may be higher than 5 GeV and it may spread up to the value of 12 GeV.

Another important variable for describing the partonic subprocess $q\bar{q} \to \gamma^* \to l^+l^-$ is the modulus of the $P^{l^+l^-}$ 4-vector, which we shall denote as "Q" and which is defined as follows:

$$Q^2 = (P_\alpha^{l^+} + P_\alpha^{l^-})^2. \tag{6}$$

It is clear from (1) that Q has the meaning of the invariant mass of two signal leptons pair, i.e.

$$M_{inv}^{l^+l-} = \sqrt{(P^{l^+l-})^2} = Q = \sqrt{(Q^2)}. \tag{7}$$

[7] This value is in an accordance with the shape of the $M_{inv}^{l^+l-}$- and $M_{inv}^{q\bar{q}}$ - distributions that are shown in the upper raw of Figure 9 . See also the Introduction and the discussion below. Note also that, according to the top raw plots of the Figure 1, the energy spectra of individual leptons in a pair may start, practically, from the zero values.

The left hand side plot in the upper raw of Figure 9 includes the distribution of the number of events versus the values of this variable (it is denoted there as "$M_{inv} - l + l - distribution''$ $(\equiv M_{inv}^{l^+l^-})$).

Let us look now at the set of variables that describe the initial quark-antiquark state of the annihilation subprocess $q\bar{q} \to \gamma^* \to l^+l^-$. In analogy with (1) one may consider the 4-momentum of $q\bar{q}$ system

$$P_\alpha^{q\bar{q}} = P_\alpha^q + P_\alpha^{\bar{q}}, \tag{8}$$

and construct with its help the variable of the invariant mass of quark-antiquark system $M_{inv}^{q\bar{q}}$ (in PYTHIA it is named as "$\hat{m}$"). Thus,

$$M_{inv}^{q\bar{q}} = \sqrt{(P^{q\bar{q}})^2} = \hat{m}. \tag{9}$$

Its distribution is shown in the right hand plot of the same first raw of Figure 9 ("$M_{inv} - qqbar \;\; distribution''$ $(\equiv M_{inv}^{q\bar{q}})$).

Both of the considered here invariant mass distributions, i.e. $M_{inv}^{q\bar{q}} = \hat{m}$ and $M_{inv}^{q\bar{q}} = Q$, look very similar. From the plots of Figure 9 it is seen that the most of events are concentrated near the starting point $M_{inv}^{l^+l^-} = 1$ GeV and there are, practically, no events after the point $M_{inv}^{l^+l^-} = 2.5$ GeV. So, the spectra of the invariant masses of produced quark-antiquark system as well as of lepton pair are rather narrow. The appearance of the left boundary points $M_{inv}^{l^+l^-}/min = M_{inv}^{q\bar{q}}/min = 1$ GeV stems from the internal PYTHIA restriction (see the discussion above and the Introduction) for the lowest value of invariant mass of two body system produced in fundamental quark-parton level $2 \to 2$ subprocess.

The distributions of Bjorken x-variables are shown in Figure 10 for up- and antiup-quarks (top raw) and for down- and antidown- quarks (bottom raw) correspondingly. They represent the up- and antiup- quarks components of the proton structure function.

The number of entries in these plots reflects the valence quark flavor structure of the proton (the analogous distributions and the number of entries for the antiquarks, given in Figure 10, show the absolute similarity of quark and antiquarks distributions, obtained from the generated PYTHIA samples).

4 The remarks on the possibility to measure the size of the intrinsic quark transverse momentum in the proton and on the role of the initial state radiation.

Now let us consider, following [12]-[14] and in a complete analogy with the equations (4)and (5), the vector sum of quark and anti-quark transverse momentum vectors

$$\vec{P}_T^{q\bar{q}} = \vec{P}_T^q + \vec{P}_T^{\bar{q}}. \tag{10}$$

and the modulus of this vector sum

$$P_T^{q\bar{q}} = |\vec{P}_T^{q\bar{q}}| = |\vec{P}_T^q + \vec{P}_T^{\bar{q}}|. \tag{11}$$

The last variable has a distribution (see right hand side bottom corner of the Figure 9 where it is denoted as "PT-qqbar-*distribution*"($\equiv P_T^{q\bar{q}}$) which shape practically coincides (in accordance with the transverse momentum conservation law) with the shape of the distribution of the number of events versus the lepton pair transverse momentum $P_T^{l^+l^-}$, shown in the left bottom corner.

The variable $P_T^{q\bar{q}}$ is of a special interest because it contains an important information about two physical features of quark dynamics inside the hadron [8]. Really, in our case when a beam antiproton moves along the z-axis and scatters off the proton fixed target (we neglect the effect of target drops transverse motion) the only sources of transverse motion of quarks [9] may be as follows:

a) quark internal Fermi-motion (with some transverse velocity) inside a proton, i.e. the so called " $k_T - effect$" ;

b) initial state radiation (ISR) of gluons (or photons) from quarks before hard quark-antiquark annihilation.

The importance of these two mentioned above effects was recently discussed in a number of papers devoted to the study of "$\gamma + jet$" events at LHC [12], [13] and Tevatron [14]. A lot of attention was paid to this problem also in [15] in connection to the interpretation of direct photons production study in the experiment E706 at Fermilab [11].

In the absence of these two sources the initial state quark and antiquark (from the colliding antiproton and proton, respectively) should have zero transverse momenta. Here we have used the possibilities of PYTHIA generator which allow to switch "on/off" each of "a)"- and "b)"- effects separately as well as to switch them "off/on" simultaneously. Let us remind (see Section 2) that both plots in the third raw of Figure 9 are done for a case when "a)-effect" (i.e. "Fermi motion" or "k_T-effect") as well as "b)-effect" (or ISR) were switched "on"(i.e., we have chosen the parameters $MSTP(91) = MSTP(61) = 1$). [10] .

Firstly we have checked that in a case when both sources a) and b) were switched "off" the corresponding plots for $P_T^{l^+l^-}$($\equiv$" $PT-l+l-$ distribution") and $P_T^{q\bar{q}}$($\equiv$ "$PT-qqbar-$ distribution") really show zero in their distributions (the initial state quark and antiquark have zero transverse momenta and thus they may produce a lepton-antilepton pair in which the leptons may have either zero or back-to-back transverse momenta). Therefore, any deviation from zero of the *total transverse momentum of a lepton pair*, produced in a hard quark-antiquark annihilation, may appear only due to the presence of one of the two mentioned above features "a)" or "b)' of quark dynamics, or as the simultaneous result of both of them.

To study the influence of ISR-effect we have switched it "off" (i.e. we set MSTP(61)=0) while keeping the parameter of Fermi motion, i.e. "k_T-effect", to be switching "on",

[8] see [12]-[14] (it was denoted there as VPT56).

[9] the transverse motion of the constituents of a target proton (which is at rest) as well as of those inside a beam antiproton (which moves along z-axis) is invariant under boosts transformations along the z-axis.

[10] Let us note also that sometimes in the literature the both of these features appear under one and the same name of "k_T-effect" (see, for instance, [15]).

(i.e. MSTP(91)=1). No difference (in the shapes as well as in the mean values) was found between the plots for $P_T^{l^+l^-}$ ("$PT-l+l-distribution''$) and $P_T^{q\bar{q}}$("$PT-qqbar-distribution''$), obtained in this case (when only the effect of Fermi motion or "k_T-effect" was taken into account) with the previously discussed plots shown in the lowest raw of Figure 9 done with the account of both effects (MSTP(91)=MSTP(61)=1). [11]

So, one may conclude that, within PYTHIA simulation, switching "on/off" of the initial state radiation does not produce any effect on the total lepton pair transverse momentum at the chosen beam energy (14 GeV). This result may indicate (still keeping in mind that this feature is based on the ISR model used in PYTHIA, i.e., it has a model nature) that the phase space limitations at the chosen value of beam energy $E_{beam} = 14$ GeV may allow to measure at PANDA the Fermi motion effect separately from the ISR effect. Further study in this direction is necessary, of course. Thus, future measurements of the total transverse momentum $P_T^{l^+l^-}$ of the lepton pairs at PANDA energies may be of a big interest for a proper treatment of many QCD results from LHC (and Tevatron) as well as by itself.

To this reason we may suppose that the fraction of events that have the final state consisting of a $l\bar{l}$-pair and a pair of two charged pions (see also the discussion in the following Section) may be the most suitable for the measuring of the primordial "k_T-effect" (caused by the intrinsic Fermi motion of quarks inside the proton) by measuring of the total transverse momentum of the lepton-antilepton pair in the final state.

5 Fake muons from hadron decays in signal events.

The signal events, defined by $q\bar{q} \to l^+l^-$ subprocess, should contain also some hadrons in the final state. The pions, produced directly or in the decays cascades of other hadrons, may decay in the detector volume and thus serve as a main source of background muons that may fake the signal muons, produced in the annihilation subprocess.

Figure 11 includes (like in the Figures 1 and 2) the distributions (from top to bottom) of the number of events versus the energy $E_{PI}= E_\pi$, the transverse momentum $PT_{PI} = PT_\pi$ and versus the polar angle $TETA_{PI}= \theta_\pi$ of produced pions.

The right hand side bottom plot contains the distribution of the total number (NPI) of charged π-mesons in the signal events. One may see from this plot that there is a big number of signal events (about 42%) which do not contain any charged pions at all (their final states mostly include the nucleon-antinucleon pairs).

This result is rather interesting. Let us underline that PYTHIA provides a good (at least one of the bests if not the best one) but still a model approximation [12] to the hadronization effects that take part in a reality. The right hand side plot of Figure 11 indicates that it may happen so that about of 40% of events with signal muon pairs may

[11] This may mean that there is not enough volume of phase space left for the initial state radiation at the chosen value of beam energy.

[12] due to the fact of up to now absence of a complete physical and theoretical understanding of parton to hadrons fragmentation processes.

appear practically without any additional fake decay muons content.

From the same right hand side plot we also see that about of 25% of events have only one charged pion in the final state (appearing mostly from Δ resonance decays) and a bit less than 25% of events may have two charged pions. It demonstrates also that about of 5% of events may have 3 charged pions and there may be about of 1.5% of events with 4 final state charged pions.

Figure 12 contains the plots with the fake muon distributions in signal muon events. Its left column includes, respectively, from top to bottom, the energy E^{μ}_{dec}, transverse momentum PT^{μ}_{dec} and polar angle θ^{μ}_{dec} distributions for muons that appear from hadrons (mostly charged π -mesons) decays. The shapes of distributions follow the analogues spectra of parent pions, presented in Figure 11. By comparing of these plots with those from signal muon pairs (see Figure 1), one may conclude that the mean value of the energy of signal muons $< E^{mu} >$ =2.6 GeV corresponds to the point in the energy distribution of fake decay muons where the contribution of fake muons (in the same signal events) is already very low. Analogously the mean value of the PT- distribution of signal muons PT^{mu}_{signal} = 0.7 GeV (see Figure 1) do corresponds to the point where the spectrum of PT^{mu}_{dec} practically vanishes .

The E- and PT- spectra of decay fake muons are rather similar to those of "slow " muons from Figure 2, but a bit softer than the last ones. They are shifted by 300 MeV (i.e. by 30%) to the left (see their mean values) as comparing with those of signal "slow" muons. Analogously the fake decay muons polar angle spectrum is shifted also to the left by 30%, i.e. by 16^o. Still, due to a big similarity of "decay" and "slow" signal muons the former may appear as a serious background.

Therefore a reasonable cut upon the muons energy E^{mu}_{dec} (see discussion in Section 2) as well as on the PT^{mu}_{dec} value may lead to an essential reduction of the decay mesons contribution and allow to keep the main part of signal events. Thus, a cut $PT^{mu}_{dec} > 0.2$ GeV may allow to get rid of a half of decay mesons in the signal events.

Another way to discriminate up to a some level the signal muons from the "decay" ones may be connected with the use of the information about the position of the fake muon production vertex. The right hand side column in Figure 12 contains (from top to bottom) the Vx-, Vy- and Vz- (i.e. along the beam direction) components of the 3-vector that defines the position of the fake muon production vertex, obtained, as everything at the PYTHIA generator level of simulation, for a space that is free of the detector equipment. The distances at these distribution plots are given in millimeters (mm). Therefore, one may see that the tails of the Vz-distribution may expand up to 100 meters (82% of events have $Vz < 100$ m) [13], while those that are along x- and y- axises practically do finish at the 20 meters distance. From these right hand plots it is clearly seen that in a case of the signal events that do include the "decay" fake muons (58% of all events) the account of the real size of the detector "decay volume" may strongly reduce the number of charged π-mesons, that potentially may produce muons in the decays, [14]

[13]the "Overflow = 1.828E+04" shows that in about of 18% of events the decay muons may appear even at more larger than 100 m distances.

[14]because at large distances the most of parent pions should interact with the material of the detector

To this reason, one may expect that in the real experimental conditions the situation with the contribution of the additional "decay" fake muons in signal events may turn out to be even much more easier. Only 25% of events have the position of Vz-component (as it may be seen from the right bottom plot of Figure 12) within the PANDA detector volume, i.e. $V_z < 10$ m. At the same time it is also seen that in about of 5% of events the Vz componet may be very close to zero. The corresponding fake muons produced near the interaction point may pose the most difficult background. Thus the detailed GEANT simulation, which is in our nearest plans, should allow to get more definite predictions about the decay mesons contribution to the background in signal events. The contribution of the background muons from the other type of events (QCD mainly) should be discussed in the following Section.

6 Lepton distributions in QCD background events.

In this Section we consider the distributions of leptons that may be produced in other than QED $q\bar{q} \to l^+l^-$ subprocesses. For this aim the generation of 100000 events was done with the use of more than 20 QCD subprocesses (including the signal $q\bar{q} \to l^+l^-$ subprocess) that exist in PYTHIA. The results have shown that the main contributions come from the events that include the following (presented in the decreasing order of $p\bar{p} \to X$) partonic subprocesses:

- $q + g \to q + g$

  (gives 50% of events and the corresponding value of cross section $\sigma = 4.88$ mb);

- $g + g \to g + g$

  (gives 30% of events and the corresponding value of cross section $\sigma = 2.96$ mb);

- $q + q' \to q + q'$

  (gives 18% of events and the corresponding value of cross section $\sigma = 1.75$ mb);

- $q + q' \to g + g'$

  (gives 0.6% of events and the value of cross section $\sigma = 5.89E - 02$ mb);

The signal $p\bar{p} \to l^+l^- + X$ processes, that includes the QED partonic subprocess:

- $q + \bar{q} \to l^+ + l^-$

components.

has the value of $\sigma = 1.72E-05$ mb what explains its very small contribution into the total number of generated events: there is only one event of this kind has appeared among 100 000 of generated events.

The shapes of the distributions of muons, produced in the mentioned above generated background QCD events (see left column of Figure 13 in Appendix) are not so much differ (what is natural) from those of fake "decay" muons produced in the signal $p\bar{p} \to l^+l^-$ processes, shown in Figure 12. The main difference appear in the number of entries: for the 100 000 of generated background events there are 3.3 times more entries for muons (335372), i.e. there are, on average, about of 3 muons (that mostly appear from pions decays) per one QCD background event. It means that the probability of appearing of a muon pair with the different signs of their charges (like in signal events) is a rather high one in QCD background events. So, they may fake quite well the signal events.

The distribution plots for the production vertices of background muons are shown in the left column of Figure 13. From the left column bottom plot of Figure 13 it is seen that in about of 75% of events there are $V_z > 10$ meters. [15] Thus, in these events the potential parent hadrons definitely should not produce muons within the volume of PANDA detector. At the same time one may see that for a lot of events the muon production vertices are rather close to the interaction point: in about of 0.5% of events the values of Vz are practicaly equal to zero and on total about of 5% of events have $V_z < 1$ metre and 25% of events have $V_z < 10$ metres. So, these fake decay muons may be separated from the signal muons latter on at the level of full GEANT simualtion with account of real detector conditions if, firstly, the information from the tracker [16] or latter on (and what is more likely may happen) the information from the calorimeter should allow to identify the muon parent particles as hadrons. [17] So, it seams that the separation of QED signal and QCD background events would be a rather hard problem for the muon channel and a more detailed GEANT simulation of muon processes with an account of the real detector conditions (material volume and the magnetic field) would be needed.

Now let us turn to the situation with the background for the electron production processes. The distributions for the electrons, produced in 100 000 of generated signal events based on the $q\bar{q} \to e^+e^-$ subprocess, are presented in the Figure 14 of Appendix. From the number of entries one may see that, on average, the enters number of fake electrons is 105283, i.e. close to muon case (see Figure 12). The analysis of the generated event listings has shown that about of 50% of generated signal events have no other electrons than those produced in signal e^+e^- pairs. In the most of other events the electrons are produced in muon decays. Some electrons do appear also as the Dalitz pairs, i.e. from the process of neutral pion decays $\pi^0 \to e^+e^-\gamma$. These pions in their turn

[15] see "Overflow is 2.449E+05" in the right bottom plot of Figure 13.

[16] the ideal situation would be if the tracker should allow to discriminate between the pion or muon tracks. It is also supposed that the problem of matching the information from the tracker with the information from the muon system would be solved.

[17] the parent hadrons of muons, which production vertices may enter the detector components volume, may give the hadron showers in a detector material before they may decay into muons. Thus, all the tracks that are pointed in the direction of fired calorimeter cells should be excluded.

may appear from the decays of η and ω mesons or from more heavy mesons or barions, produced as the resonance states according to the LUND fragmentation model. Due to the fact that the life time of these resonance states is rather short, this kind of electron pairs are produced practically at the interaction point, what is reflected in the right hand side column of Figure 14, that contains the values of the components of the vector of the production vertex position. This fact shows some disadvantage of e+e- channel as comparing with muon one where the most of background muons were coming from the light charged pions decaying in flight at rather large distances from the interaction point. But it does not mean that the vertex position information turns not be so efficient for separation of signal and background electron events as comparing to the background muons case.

Really, as it is seen from the right hand side bottom plot for the Vz-component of the vector of the fake electron vertex position, only less than 2% of fake electrons are produced near the interaction point position $V_z = 0$. About of 97% of events have the value $V_z > 10$ metres ("Overflow = 1.001E+05"), i.e. most likely are produced from the decays of fast muons (less energetic muons may give about of 0.6% of fake electrons inside the $V_z < 10$ m volume of PANDA detector, as it is seen from the "Integral" value in this right corner plot).

Let us tern now to the case of electrons produced in the non-signal events. The corresponding distributions, obtained from the same sample of 100 000 generated QCD background events, are shown in Figure 15 of Appendix. From the number of entries one may see that, on average, the fraction of fake electrons in QCD background events (5487) is about of 60 times less than the analogous muons fraction (335372) (see Figure 13). This is an obvious advantage of the electron channel. From the left hand side column, that contains the values of the components of background electron vertex production position, we see that the QCD background electrons are also produced mostly at the origin, i.e. from Dalitz decays of neutral mesons like pion, η, ω and others. The number of "Overflow" events (443) may be connected with the fast muon decays out of the detector size, (i.e. with $V_z > 10$ m).

Now, taking into account that, as it became clear from the PYTHIA event listings, in QCD events the decay electrons, that are produced within the PANDA volume $V_z < 10$ m, do appear mostly in Dalitz pairs, we may estimate the fraction of QCD background events, that really may pose the background $e + e-$-pairs, as of about of 3% order. [18]

As it is seen from the background electron Energy- and PT-distributions, shown in the left hand side of Figure 15, these spectra fall much more steeply (as pion energy in Dalitz process have to be shared between 3 particles) than the analogous background muon spectra of Figures 12 and 13. To this reason the energy cut $E^{\mu} < 2$ GeV or the PT cut $PT^{\mu} < 0.4$ GeV may kill a lot of background events.

Nevertheless, these cuts may not be sufficient for the compensation of five orders difference in the rates of signal and background events for their clear separation.

A possible way to solve this task (taking into account the discussed above suppression

[18] or about of 2 orders less as comparing to the decay muon background in muon channel

of electron background in QCD events down to only 3% content in generated events) may be connected with the detector (a tracker and an electromagnetic calorimeter) possibilities of the identification of those electron pairs that may be associated with their parent decayed mesons by the reconstruction of the invariant mass of the system composed of the electron pair and of one of the registered photons, which may appear from the Dalitz decay process $\pi^0 \to e^+e^-\gamma$. This way, combined with the imposing of the cut from bellow on electron energy and its transverse momentum, may be even much more efficient in a case if the electromagnetic calorimeter possibilities would also allow to reconstruct the masses of the neutral pions from the other photon pair signals in event.

So, one may conclude from here that a more detailed study, based on full GEANT reconstruction with account of the detector conditions, would be very important for further study of electron pair production channel as well as for the muon one.

7 Conclusion.

The sample of $p\bar{p} \to l\bar{l} + X$ events , simulated by help of PYTHIA event generator with the use of the hard partonic $q\bar{q} \to l^+l^-$ subprocess, is used to make a set of 50 plots which give a reasonable, but approximate, physical picture of the lepton pair production in a case when the antiproton beam of intermediate energy $E_{beam} = 14$ GeV would scatter off the target proton.

The distributions of the most of essential kinematic variables of individual leptons, produced in the parton subprocess $q\bar{q} \to l^+l^-$, are described in the Section 2 and are presented in the Figures 1 and 2 of the Section 7 (Appendix). They show that the energy and the angle spectra of the fast (most energetic) leptons in a pair are very different from those of slow leptons: the mean values $< E^l_{fast} >= 3.86$ GeV are about three times higher than those of slow ones $< E^l_{slow} >= 1.36$ GeV. The simulation has shown also a tendency, which may be rather a general one: the fast leptons do fly predominantly at smaller angles $< \theta^l_{fast} >= 16.5^o$ as comparing to the angles of the slow ones $< \theta^l_{slow} >= 38.2^o$. It is worth to mention that about of 6% of events may have slow leptons in l^+l^- pairs that may scatter into the back hemisphere, i.e., $\theta^l_{slow} > 90^o$.

The energy-energy and angle-angle correlations among a slow and a fast lepton in one and the same lepton pair in event are also described in Section 2 and are presented in the plots of Figures 3-8 in Section 7 together with the corresponding distributions of the number of events versus the corresponding lepton energies and angles.

It should be noted that the present simulation, based on PYTHIA, does not take into account, of course, the detector effects (like the magnetic field, for example). Hence, the obtained plots, which describe the unbiased distributiond of free produced particles, may be useful as for the preliminary estimations mainly. Nevertheless, there is a big probability that the main features of the process would be similar to those presented at these plots. Thus, from the Figures 2 and 8 it is clear that one may expect that the cut $E^l > 0.5$ GeV, which is a very reasonable due to the effect of the detector material, may lead to a loss of 25% of events with signal lepton pairs, mainly due to the presence of the peak

in the slow lepton energy spectrum in this region. The data from the generated samples are planned to be used for a further GEANT simulation of these processes within the detector conditions.

The study of the 4-momentum components variables of the lepton pair system as a whole, done in the Section 3, has shown that the spectrum of the invariant mass of the lepton pair, which starts (due to the already discussed in Introduction restriction onto the value of the lepton pair invariant mass) at the value of $M_{inv}^{l^+l^-} = 1$ GeV, decreases rather fast and do vanishes at $M_{inv}^{l+l-} = 2.5$ GeV. At the same time the lepton pairs total energy $E^{l^+l^-}$ spectrum starts at around 1 GeV and spreads up to the value of 12 GeV. In Section 3 it was shown also that about a half of events do have the energy of a lepton pair higher than 5 GeV. So, in about a half of events the lepton pairs are rather energetic and they take away of more than 1/3 of the total energy of the produced l^+l^- system.

In Section 4 it was pointed out that the total transverse momentum $P_T^{q\bar{q}}$ of the annihilating $q\bar{q}$-pair may be caused, in principle, by two sources. It may appear due to the intrinsic transversal Fermi motion of quarks inside the nucleon or in a result of the initial state radiation of gluons. The results of the simulation have shown that, at least within the framework of PYTHIA simulation, the initial state radiation (ISR) gives a negligible contribution at the chosen value of energy. Therefore, it was argued that the study of the spectrum of the total transverse momentum of l^+l- pair (which coincides with the spectrum of the total transverse momentum $P_T^{q\bar{q}}$ of the annihilating $q\bar{q}$-pair due to the 4-momentum conservation law) may allow to measure the intrinsic Fermi motion of quarks inside the nucleon. The results of such a measurement may be very useful for an interpretation of many QCD processes at future experiments at LHC as well as of the data collected at Tevatron. All what was said above and discussed in the Sections 2-4 may be to a good approximation applied both to the case of $\mu^+\mu^-$ as well as to the case of e^+e^- pair production in the final state

An important question of a background is considered in Sections 5 and 6. In Section 5 we have concentrated on the additional muons that may appear from meson decays in the same signal process, defined by the mentioned above quark-antiquark annihilation to muon pair. The problem is that the spectra of "slow "muons, which are present in the signal muon pair, are very similar to those of fake "decay" muons. The most important observation, done in the Section 5, is that PYTHIA predicts that there would be about of 42% of events that would not contain at all the charged pions in the final state and thus they would be free of fake muons. It is also shown there that the information about the coordinate position of the muon production vertex, as well as the imposing of the cut on the values of E^{mu} or of PT^{mu}, may be useful for the discrimination of the fake muons.

In Section 6 the study of background lepton events is presented. It has been shown that in both muon and electron cases the separation of signal and muon background should not be a simple task and it needs more efforts. It was pointed out that the electron pair production channel has an evident advantage as been compared with the muon one. It is argued that the detailed GEANT simulation with an account of the detector design (and based on the simulated and described here PYTHIA event sample) may be very useful. The results of this simulation should be a subject of our following publications.

The authors are grateful to G.D.Alexeev for the suggestion of this topic for study, the interest to the work and multiple stimulating discussions of the questions concerned.

References

[1] V.A. Matveev, R.M. Muradian, A.N. Tavkhelidze, JINR P2-4543, JINR, Dubna, 1969; SLAC-TRANS-0098, JINR R2-4543, Jun 1969; 27p.

[2] S.D. Drell, T.M. Yan, SLAC-PUB-0755, Jun 1970, 12p.; Phys.Rev.Lett. **25**(1970)316-320, 1970.

[3] CERN UA1 Collaboration, C. Albajar et al., Phys. Lett., **B209** (1988) 397; FNAL E772 Collaboration, P.L. Gaughey at al. Phys. Rev. **D50** (1994) 3038;

[4] A.D. Martin *et al.*, Eur. Phys. J. **C4** (1998) 463.

[5] S.Okubo, Phys.Lett. B 5, 165 (1963); G.Zweig, CERN Report 8419/th 412 (1964) ; I.Izuka, Prog. Theor. Phys (suppl 37) 38 21 (1966);

[6] M.Bargiotti et al., EPJdirect A 2,1 (2002);

[7] M.Bargiotti et al., Eur. Phys. J. C 35, 177 (2004);

[8] A.N.Skachkova, N.B.Skachkov hep-ph/0412279, 2004.

[9] T.Sjostrand, Computer Phys. Commun.**39** (1986) 347, T.Sjostrand and M.Bengtsson, Computer Phys. Commun.**43** (1987)367.

[10] R. Brun and F. Rademakers, ROOT - An Object Oriented Data Analysis Framework, Proceedings AIHENP '96 Workshop, Lausanne, Sep. 1996, Nucl. Inst. & Meth. in Phys. Res. **A389** (1997) 81. See also http://root.cern.ch/.

[11] Fermilab E706 Collab., L. Apanasevich et al. Phys.Rev.D70:092009 ,2004, hep-ex/0407011; Phys.Rev.Lett.81:2642-2645,1998, hep-ex/9711017.

[12] N.B. Skachkov, V.F. Konoplyanikov D.V. Bandourin, Third Annual RDMS CMS Collaboration Meeting. CMS-Document, 1997–168. CERN, December 16-17, 1997, p.139-153.

[13] D.V. Bandurin, V.F. Konoplyanikov, N.B. Skachkov, hep-ex/0207028;

[14] D.V. Bandurin, N.B. Skachkov, D0-NOTE-3948,FNAL, Mar. 2002, hep-ex/0203003, 2002; Phys.Part.Nucl.35:66-106, 2004 (Fiz.Elem.Chast.Atom.Yadra 35:113-177,2004), hep-ex/0304010;

[15] L. Apanasevich et al., Phys.Rev.D59:074007,1999; hep-ph/9808467;
J. Huston; Int.J.Mod.Phys.A16S1A:205-208,2001;

[16] B. Andersson, G. Gustafson and C. Peterson, Z. Phys. **C1** (1979) 105;

B. Andersson, G. Gustafson, Z. Phys. **C3** (1980) 22;

B. Andersson, G. Gustafson and T. Sjostrand, Z. Phys. **C6** (1980) 235; Z. Phys. **C12** (1982) 49;

[17] B. Andersson, G. Gustafson and T. Sjostrand, Phys. Lett. **B94** (1980) 211;

[18] B. Andersson, G. Gustafson, I. Holgersson and O. Mansson, Nucl. Phys. **B178** (1981) 242;

[19] B. Andersson, G. Gustafson, G.Ingelman and T. Sjostrand, Z. Phys. **C9** (1981) 233;

[20] B. Andersson, G. Gustafson and T. Sjostrand, Nucl. Phys. **B197** (1982) 45;

[21] B. Andersson, G. Gustafson, G. Ingelman and T. Sjostrand, Phys. Rep. **97** (1983) 31;

8 Appendix: Figures.

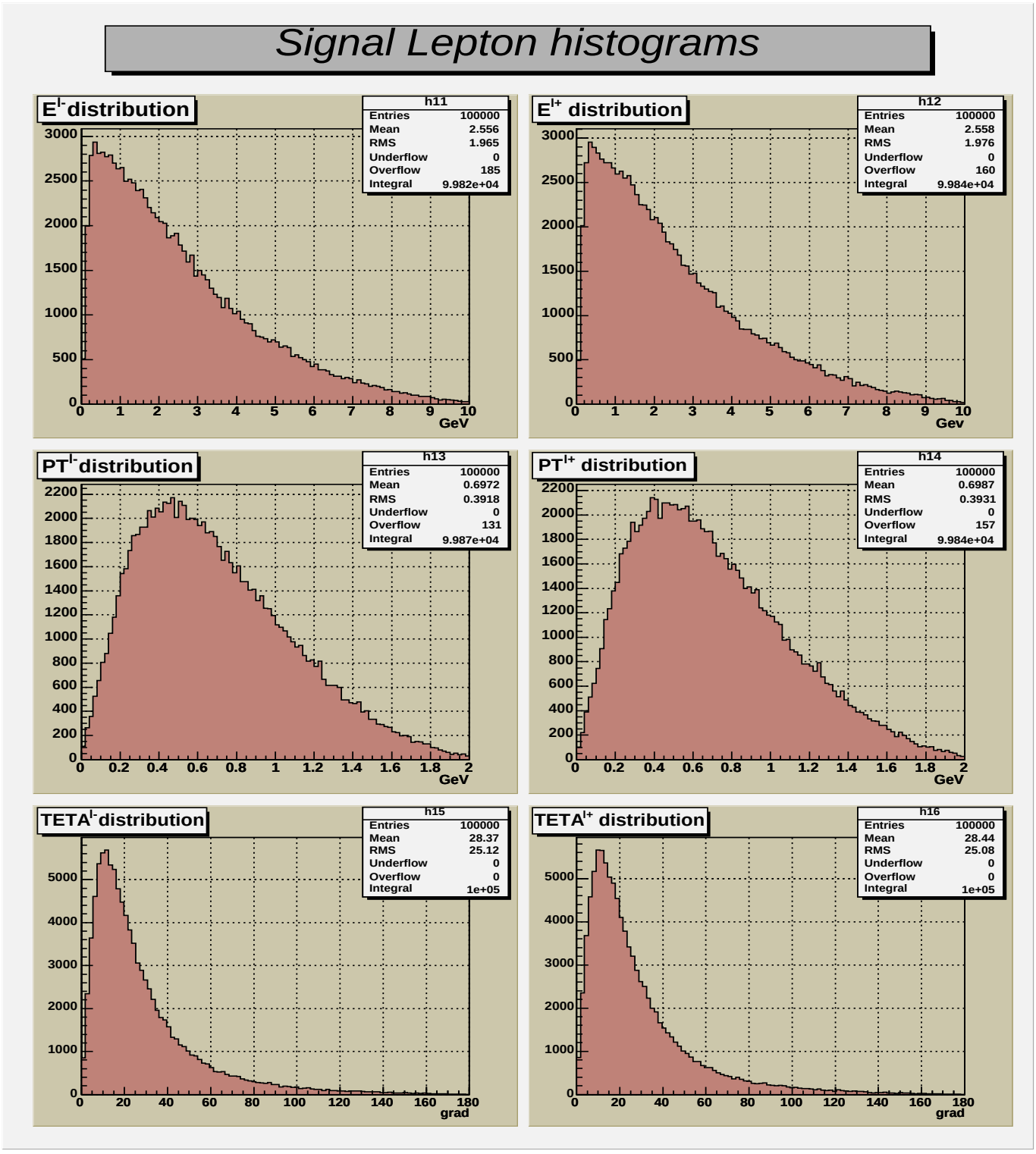

Figure 1: Signal leptons energy (in GeV) $E^{l^{(+/-)}}$ (top raw), the modulus of the transverse momentum (in GeV) $PT^{l^{(+/-)}}$ (middle raw) and the polar angle $\theta^{l^{(+/-)}}$ (bottom raw) distributions. Left column is for l^- and right one for l^+.

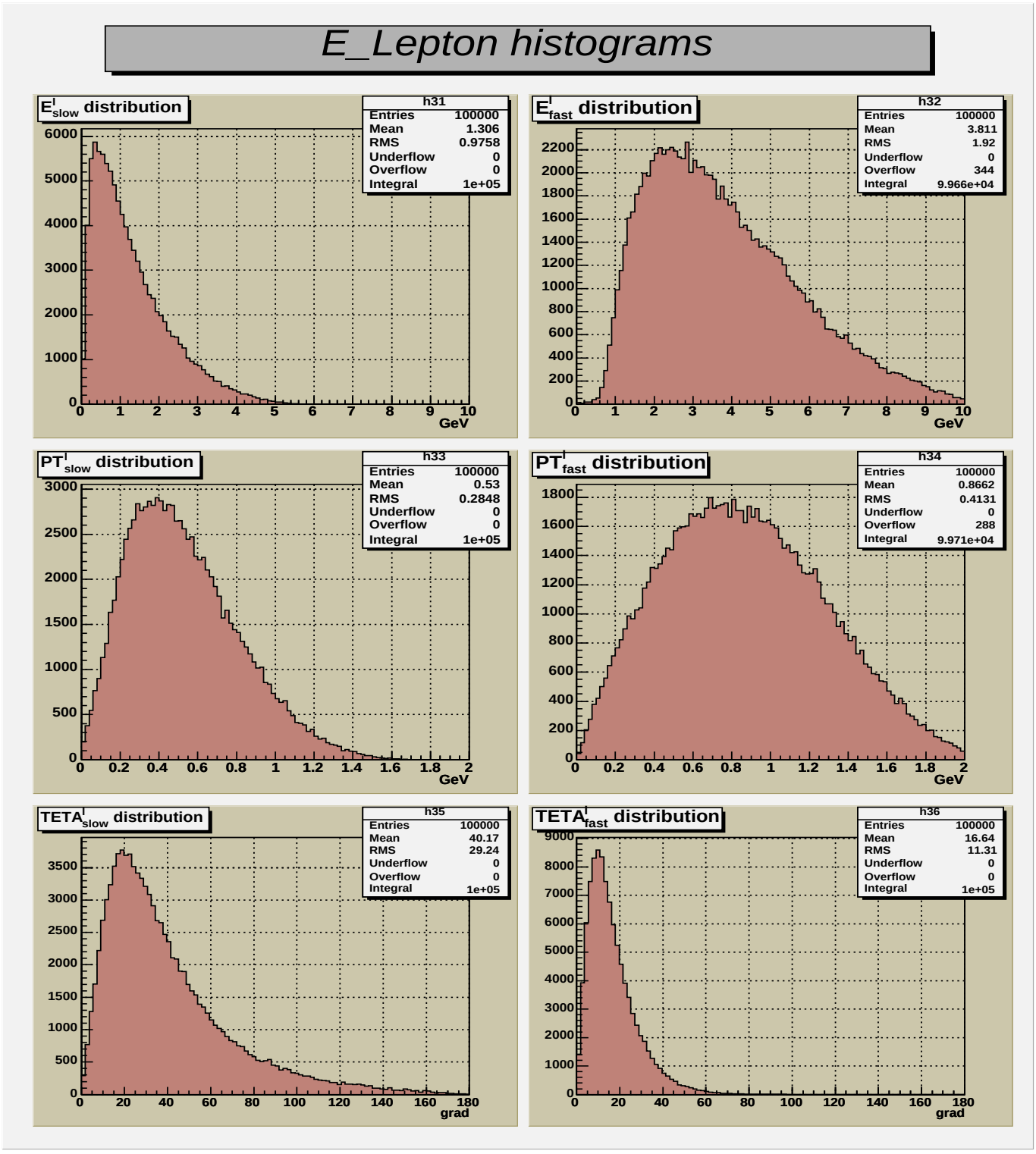

Figure 2: The analogous to Figure 1. signal distributions for leptons with the largest energy ("fast" leptons) in the lepton pair E^l_{fast} (left column) and the smaller energy ("slow" leptons) E^l_{slow} (right column). Top raw includes their energies, in middle raw are PT^l and in bottom raw are θ^l.

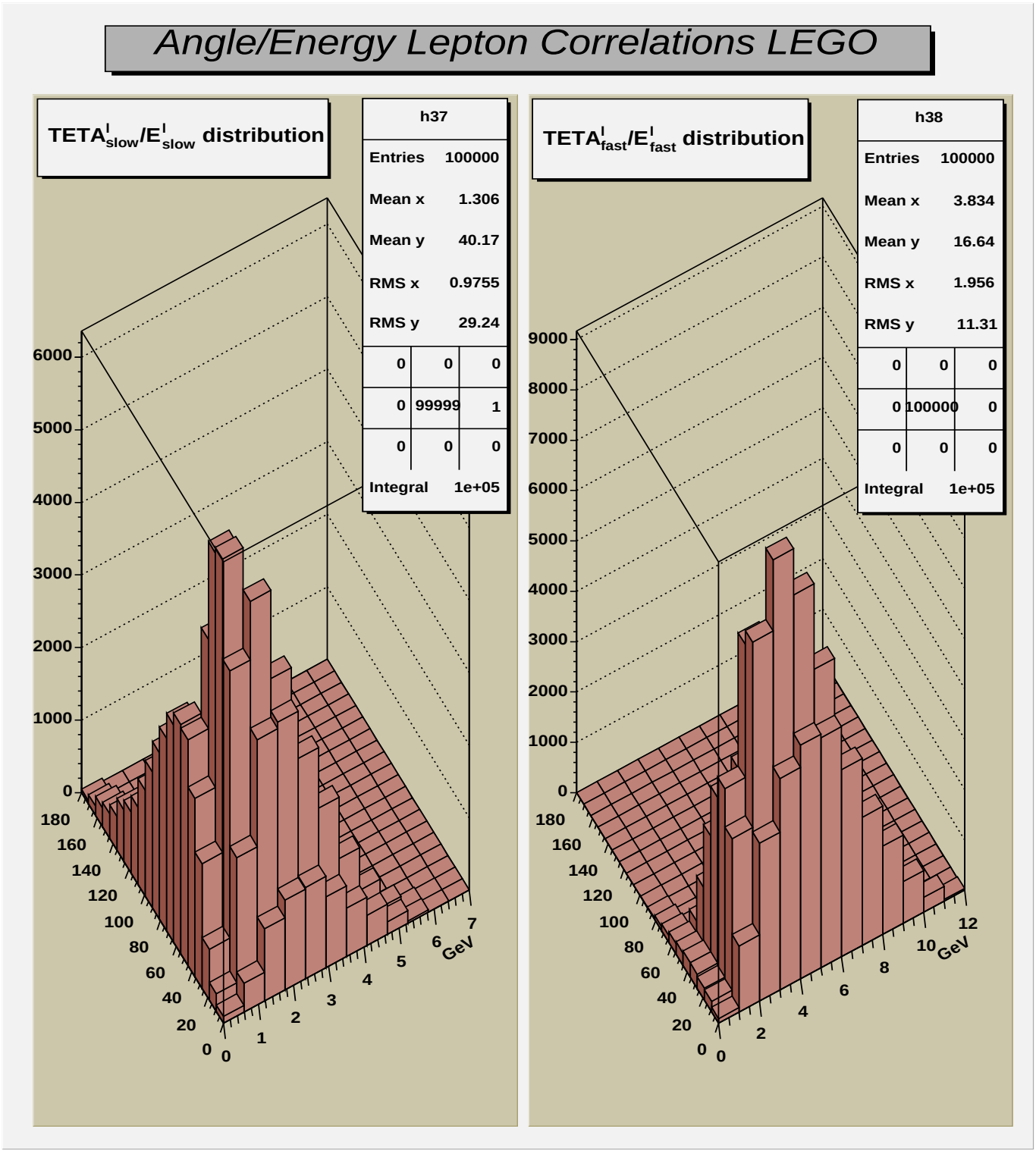

Figure 3: The "LEGO" ROOT plots for the the number of events distribution versus angle (in degrees)) and energy (in GeV) of leptons. It shows the angle/energy correlations of signal leptons in events. Left hand plot shows the correlation for "slow" leptons in event, while the right hand one for "fast" leptons.

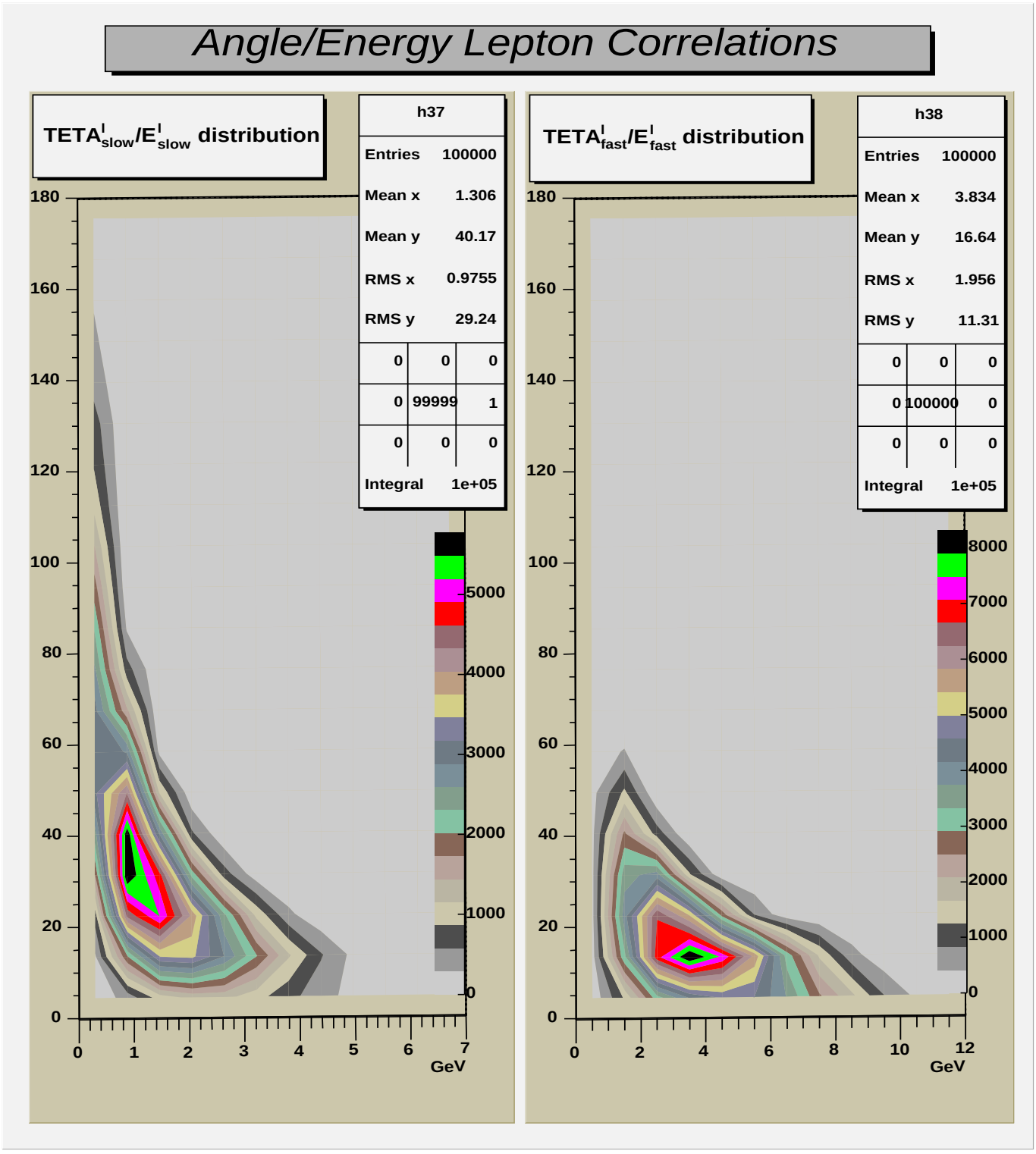

Figure 4: The "SURF2Z" ROOT plots show the same as in Figure 3 angle/energy correlations but as been projected onto θ^l/E^l plane. In each plot the right hand vertical scale shows the one-to-one correspondence between the color and the number of events per square bin (see Fig.3 "LEGO" and Fig.5 "TEXT" plots).

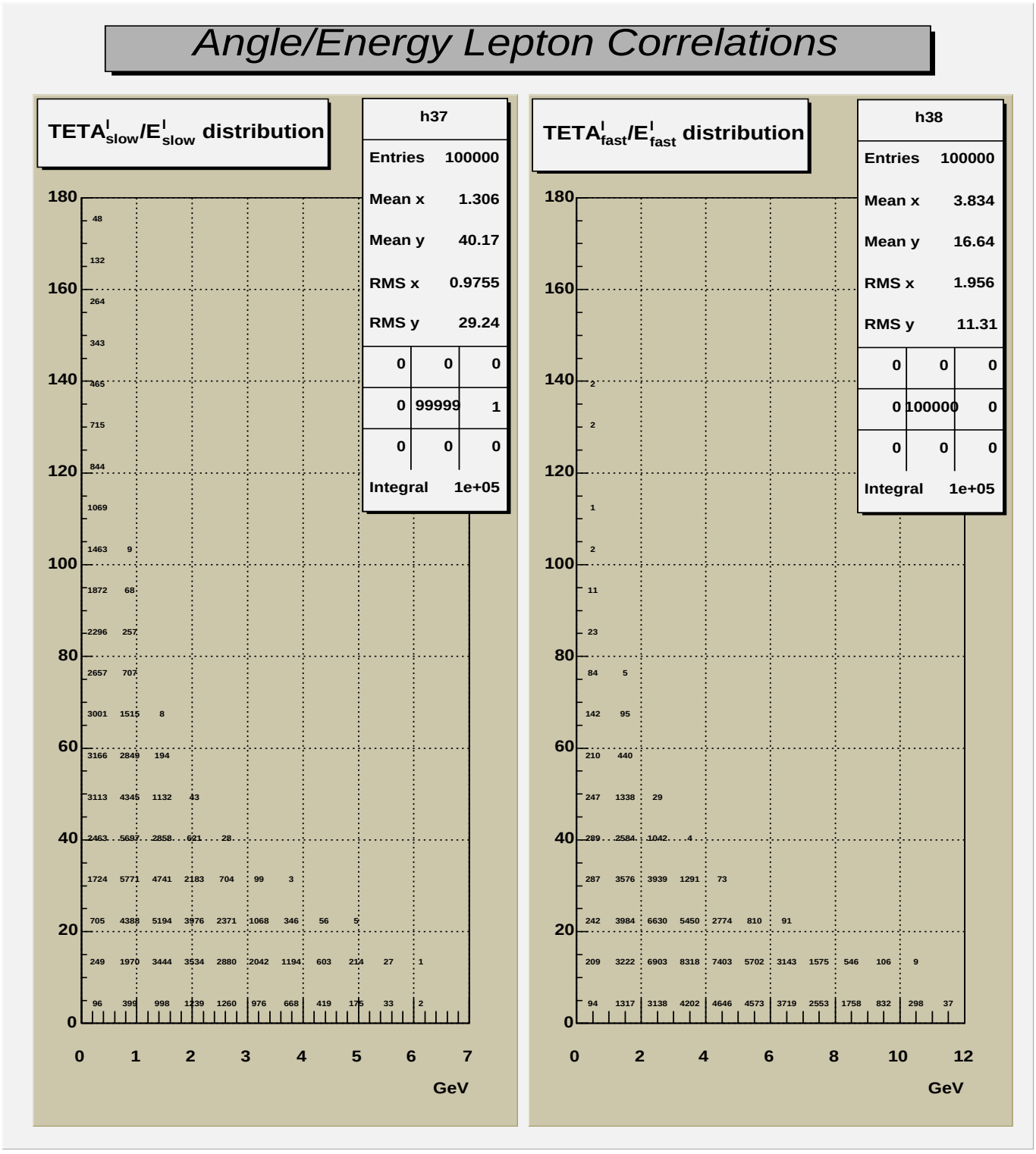

Figure 5: The "TEXT" ROOT plots show the same as in Figure 4 leptons angle/energy correlations but with the number of events per square bin (see Fig.3 "LEGO" plot and compare with Fig.4). Exact numbers in each square may be seen by help of zoom applied to .ps file plots.

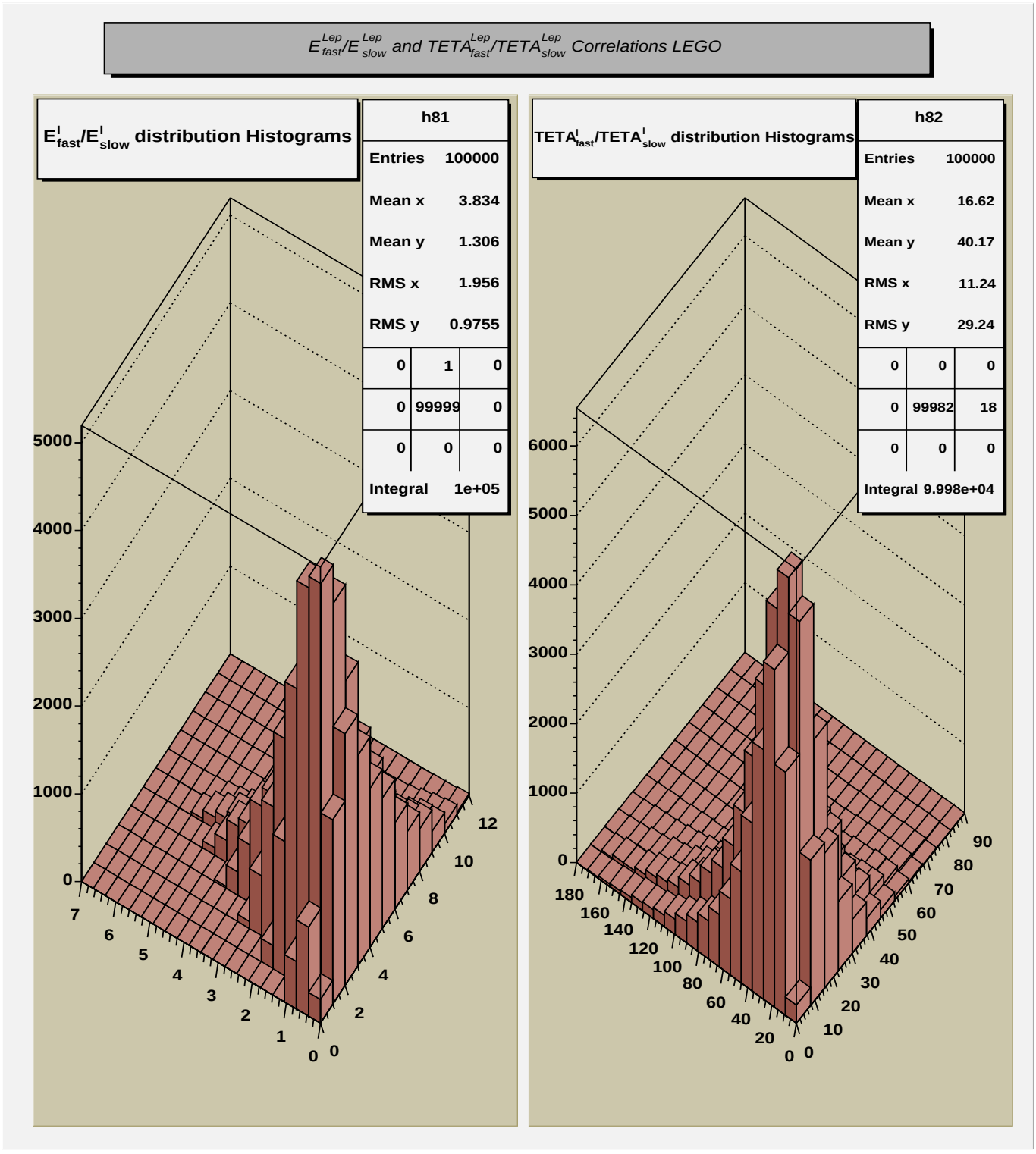

Figure 6: The "LEGO" ROOT plots for the the number of events distribution versus angle and energy of leptons. It shows the the signal leptons E^l_{slow}/E^l_{fast} (left side) and $\theta^l_{slow}/\theta^l_{fast}$ (right side) correlations in generated events.

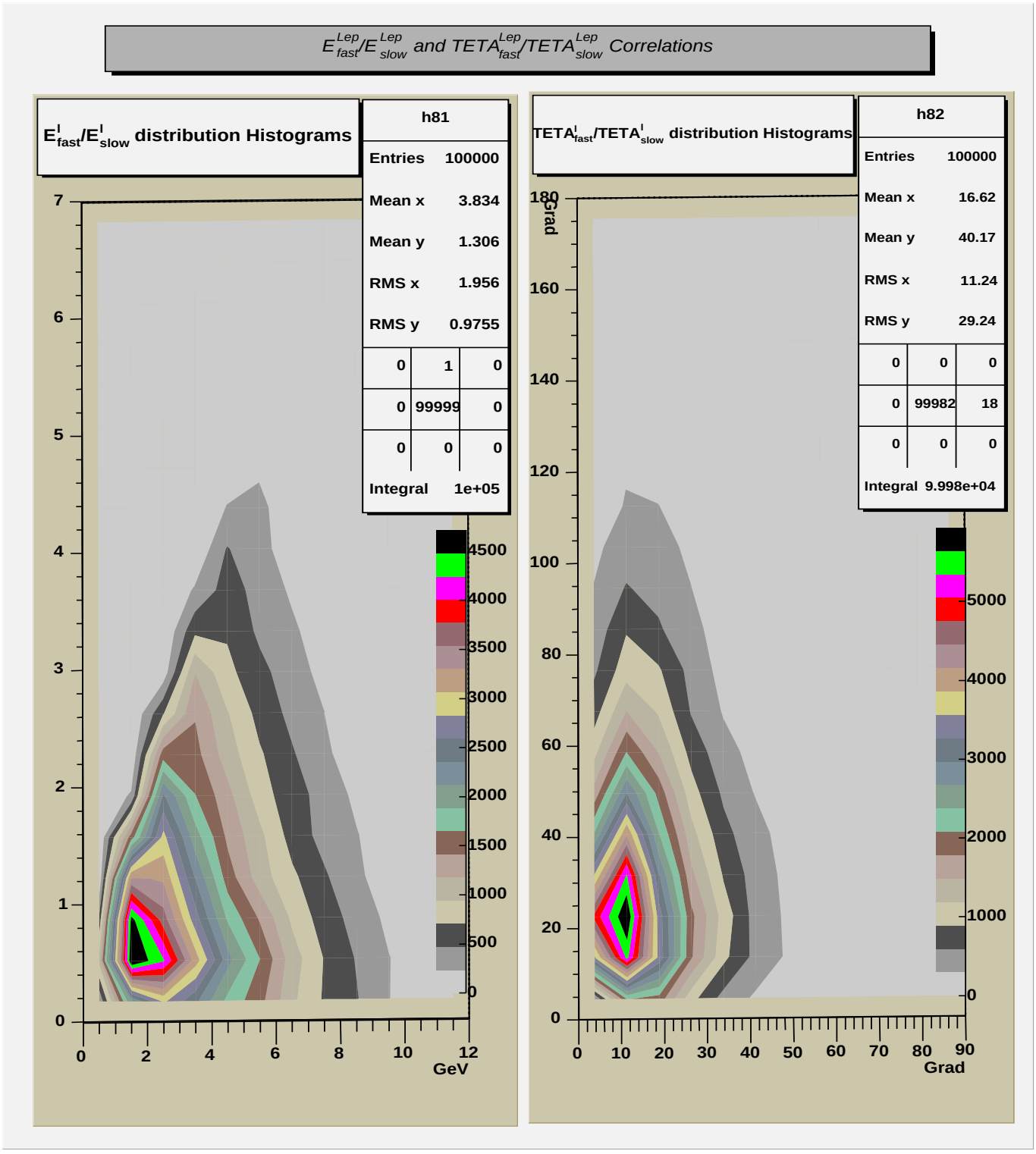

Figure 7: The "SURF2Z" ROOT plots show the same as in Figure 6 E^l_{slow}/E^l_{fast} (left side) and $\theta^l_{slow}/\theta^l_{fast}$ (right side) correlations but as been projected onto E^l_{slow}/E^l_{fast} and $\theta^l_{slow}/\theta^l_{fast}$ planes. The right hand vertical scale in each plot shows the one-to-one correspondence between the color and the number of events per square bin (see Fig.6 "LEGO" and Fig.8 "TEXT" plots).

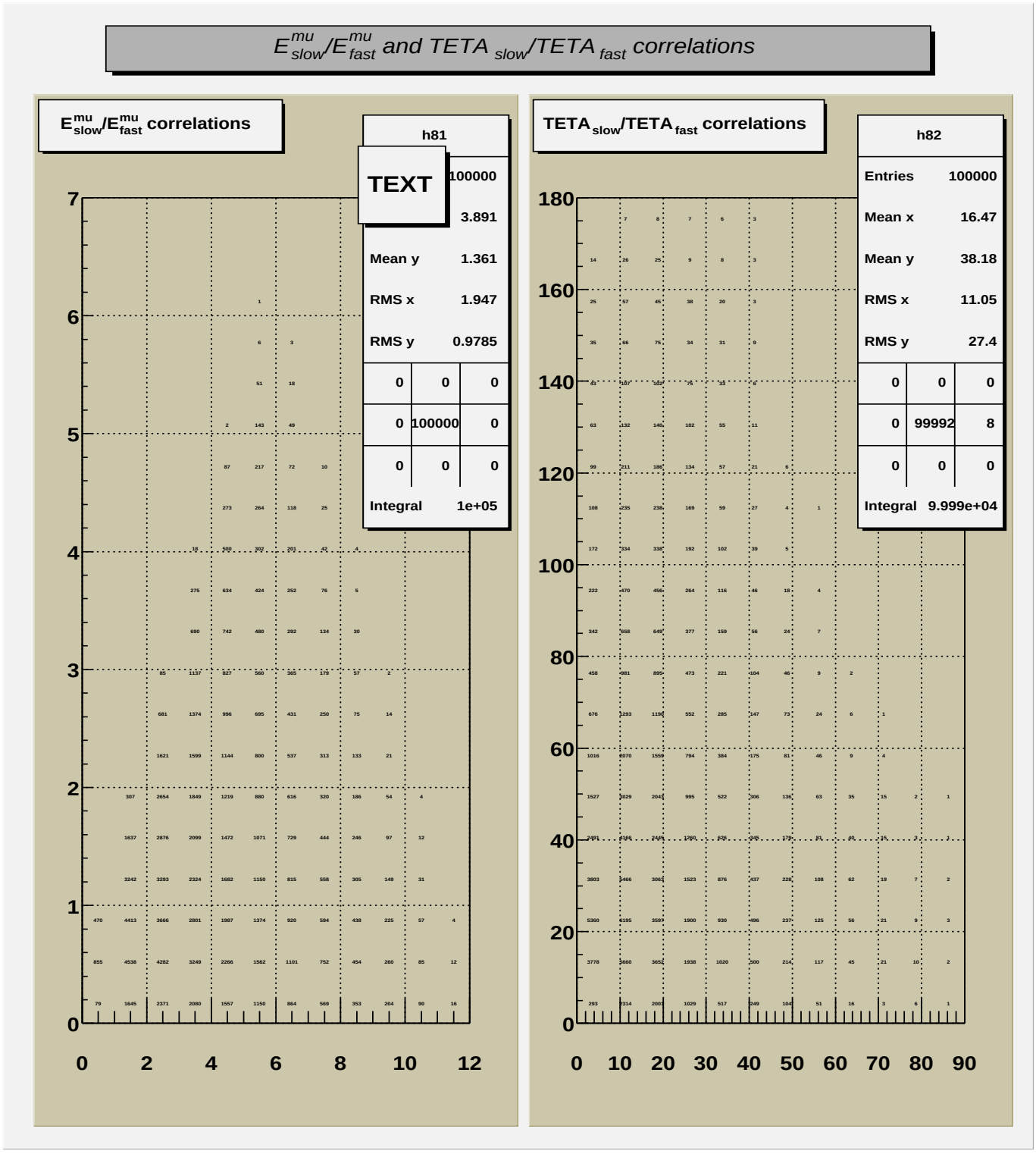

Figure 8: The "TEXT" ROOT plots show the same as in Figure 6 and Figure 7 leptons energy/energy and angle/angle correlations but presented as the number of events per each square bin (see Fig.6 "LEGO" plot and compare with Fig.7). The exact numbers in each square bin may be seen by help of zoom applied to .ps file plots.

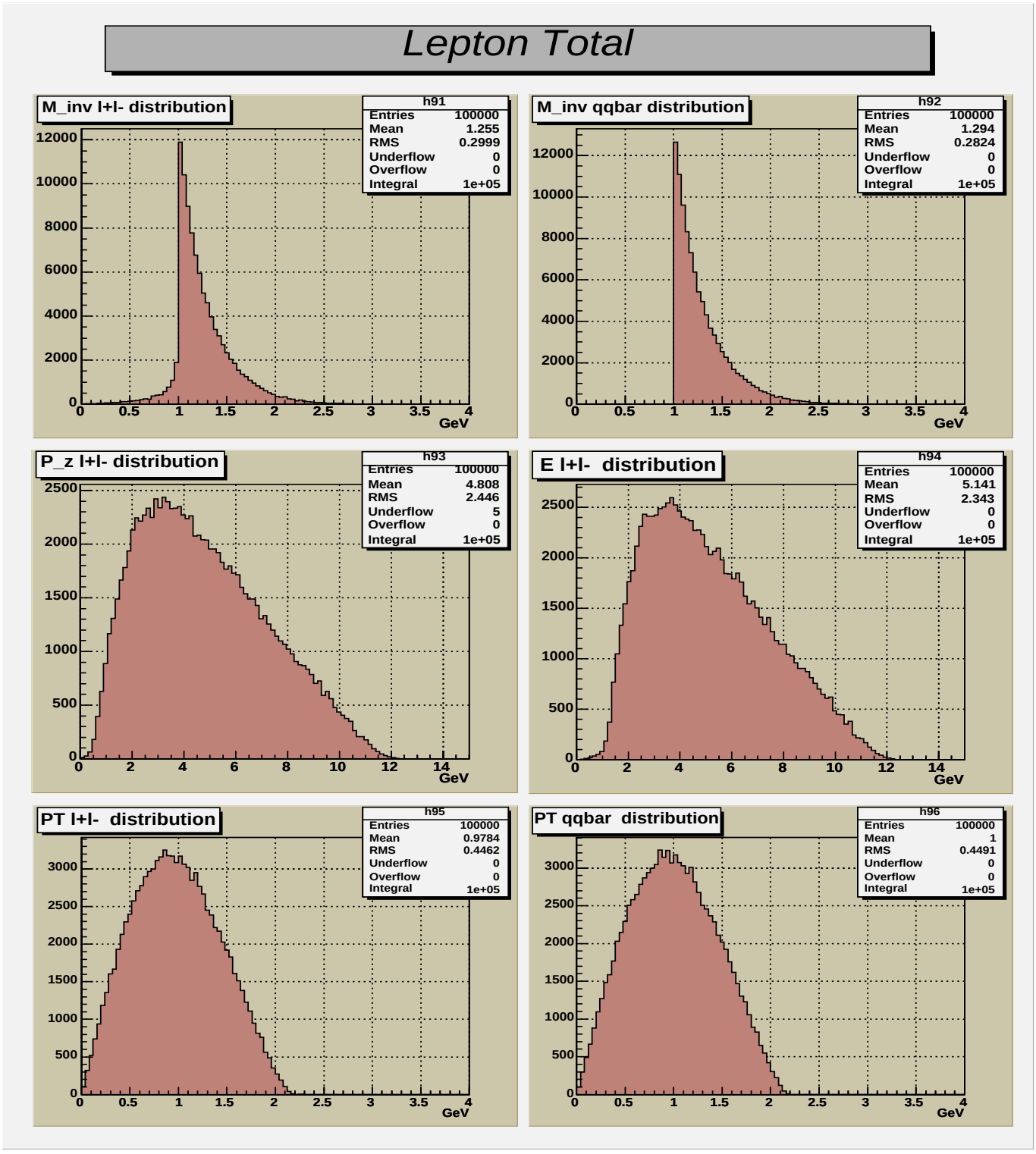

Figure 9: The upper raw includes the distributions of invariant masses of lepton pair $M_{inv}^{l^+l^-}$ (left column) and of quark-antiquark system $M_{inv}^{q\bar{q}}$ (right column) . The middle raw contains the distributions of Pz- and energy- components of l^+l- system . In the bottom raw the total transversal momenta of lepton system (left corner) and of of $q\bar{q}$ system (right side) are shown.

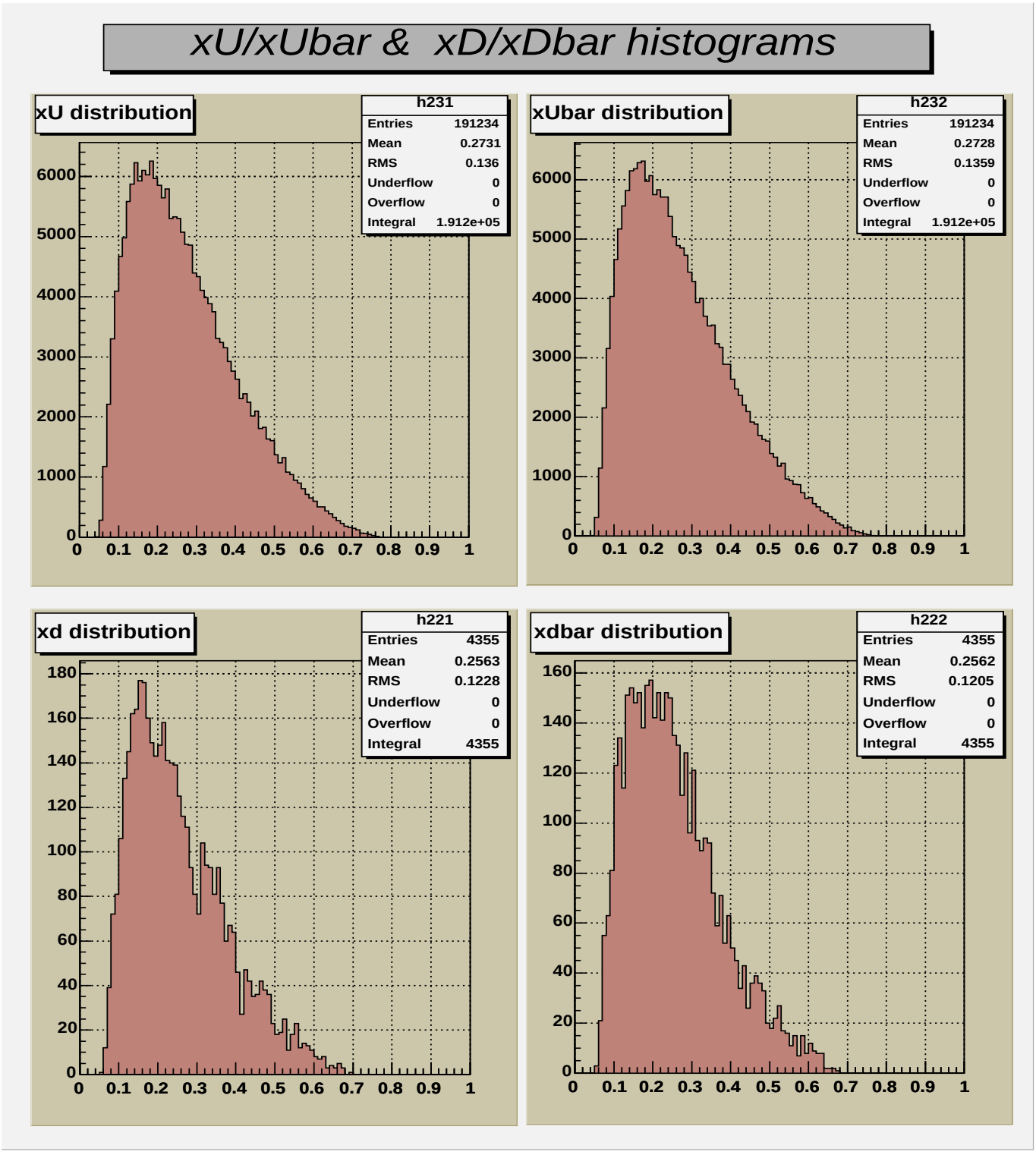

Figure 10: Top raw shows the x distributions of valence up -quarks and up-anti-quarks, while bottom raw includes the analogous distributions of down-quarks and down-anti-quarks.

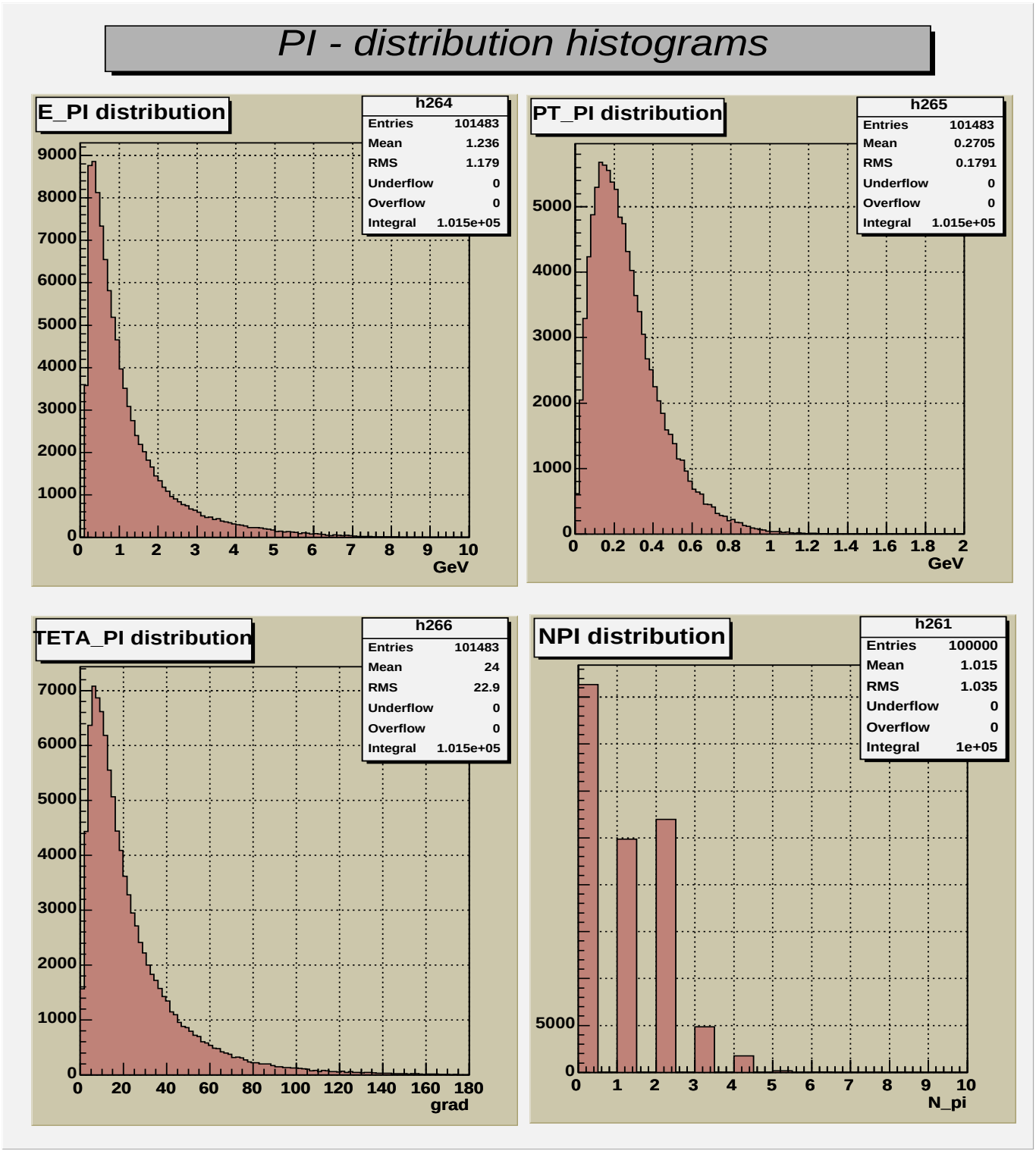

Figure 11: The left column includes the distributions (from top to bottom, respectively) of number of events versus the energy E_{PI}=E_{π}, the transverse momentum PT_{PI}= PT_{π} and versus the polar angle $TETA_{PI}$= θ_{π} of produced pions. The right hand plot shows the distribution of the total number (NPI) of charged π-mesons in the signal events.

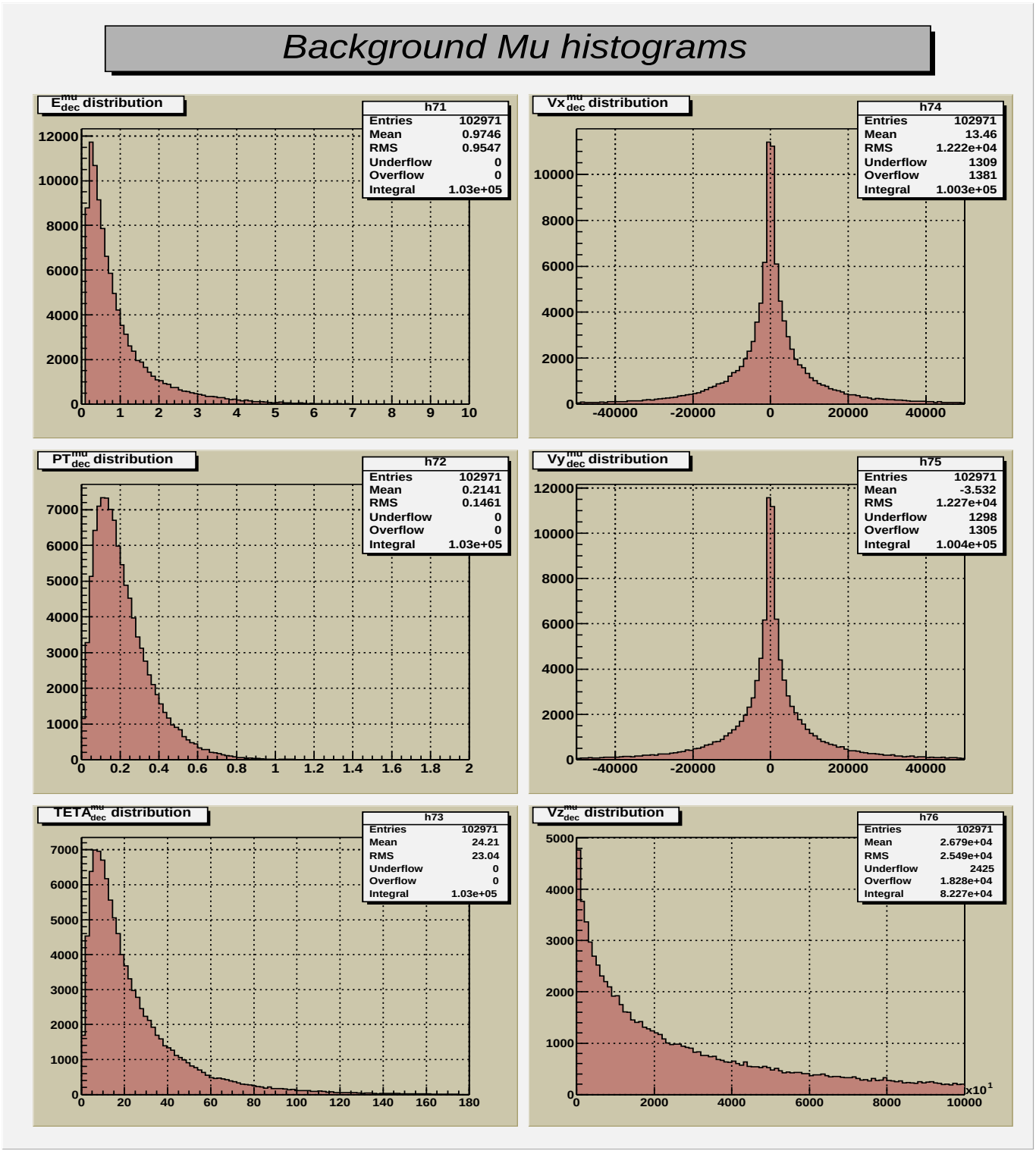

Figure 12: The left column includes the distributions (from top to bottom, respectively) of number of events versus the energy E^{μ}_{dec}, the transverse momentum PT^{μ}_{dec} and the polar angle θ^{μ}_{dec} of decay muons, produced in hadron decays in signal events that include the $q\bar{q} \to \mu^+\mu^-$ subprocess. The right column (from top to bottom) shows the distributions (in mm) of V_x-, V_y- and V_z- components of the position vector of a decay electron production vertex.

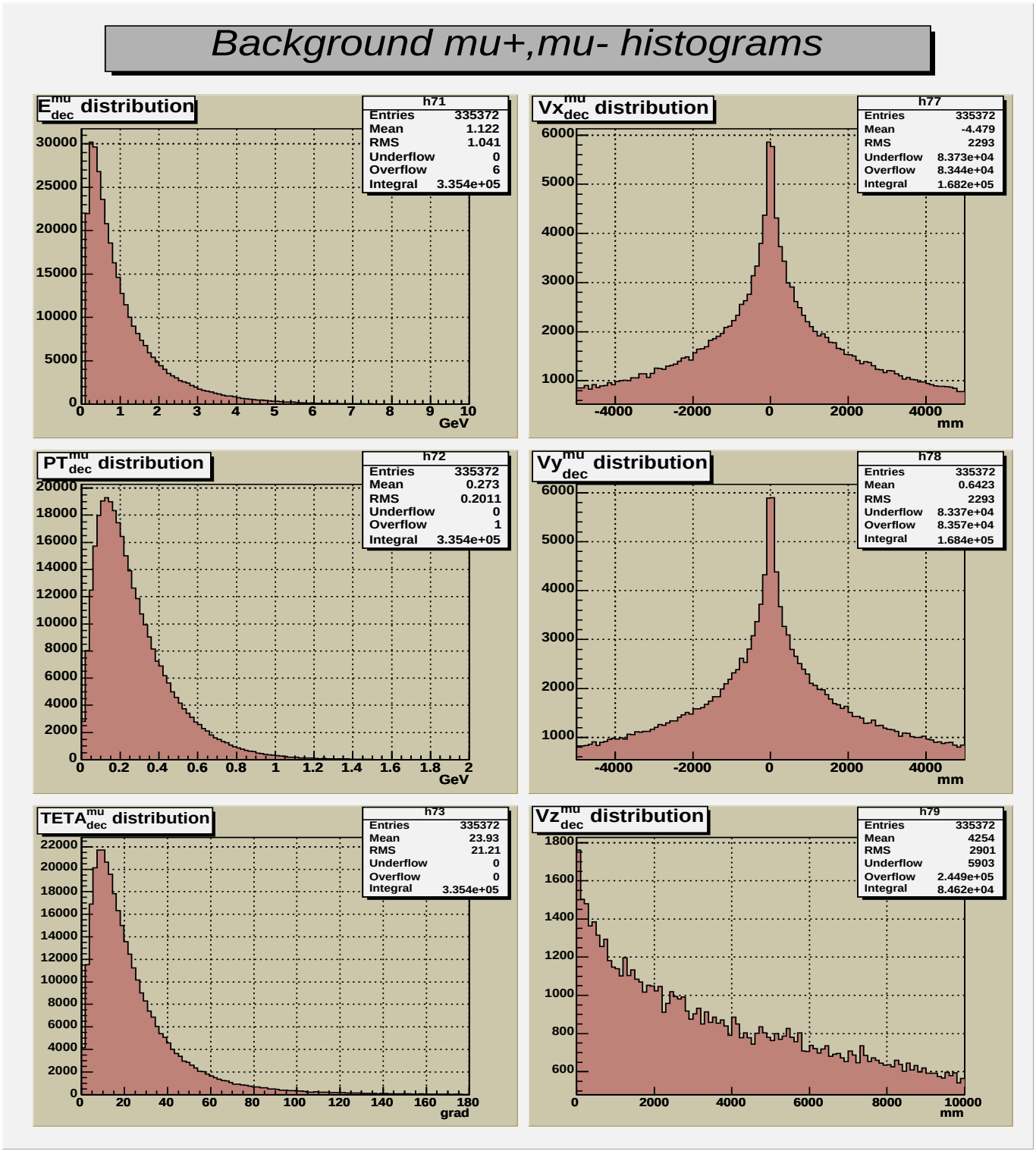

Figure 13: The left column includes the distributions (from top to bottom, respectively) of number of events versus the energy E^{μ}_{dec}, the transverse momentum PT^{μ}_{dec} and the polar angle θ^{μ}_{dec} of muons, produced in QCD background events. The right column (from top to bottom) shows the distributions (in mm) of the V_x-, V_y- and V_z- components of the position vector of a decay electron production vertex.

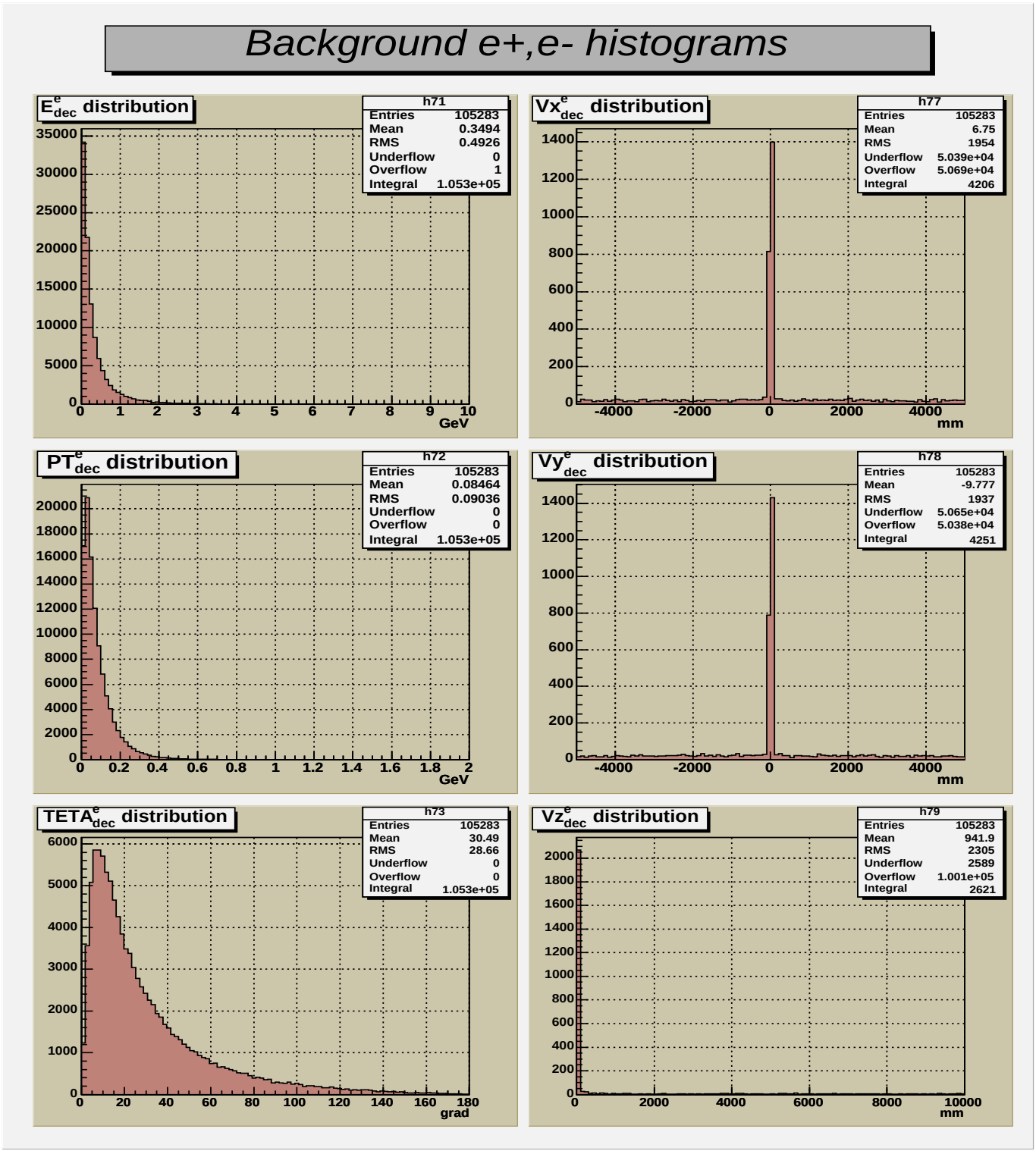

Figure 14: The left column includes the distributions (from top to bottom, respectively) of number of events versus the energy E^e_{dec}, the transverse momentum PT^e_{dec} and the polar angle θ^e_{dec} of electrons, produced in hadron decays in signal events that include the $q\bar{q} \to e^+e^-$ subprocess. The right column (from top to bottom) shows the distributions (in mm) of V_x-, V_y- and V_z- components of the position vector of a decay electron production vertex.

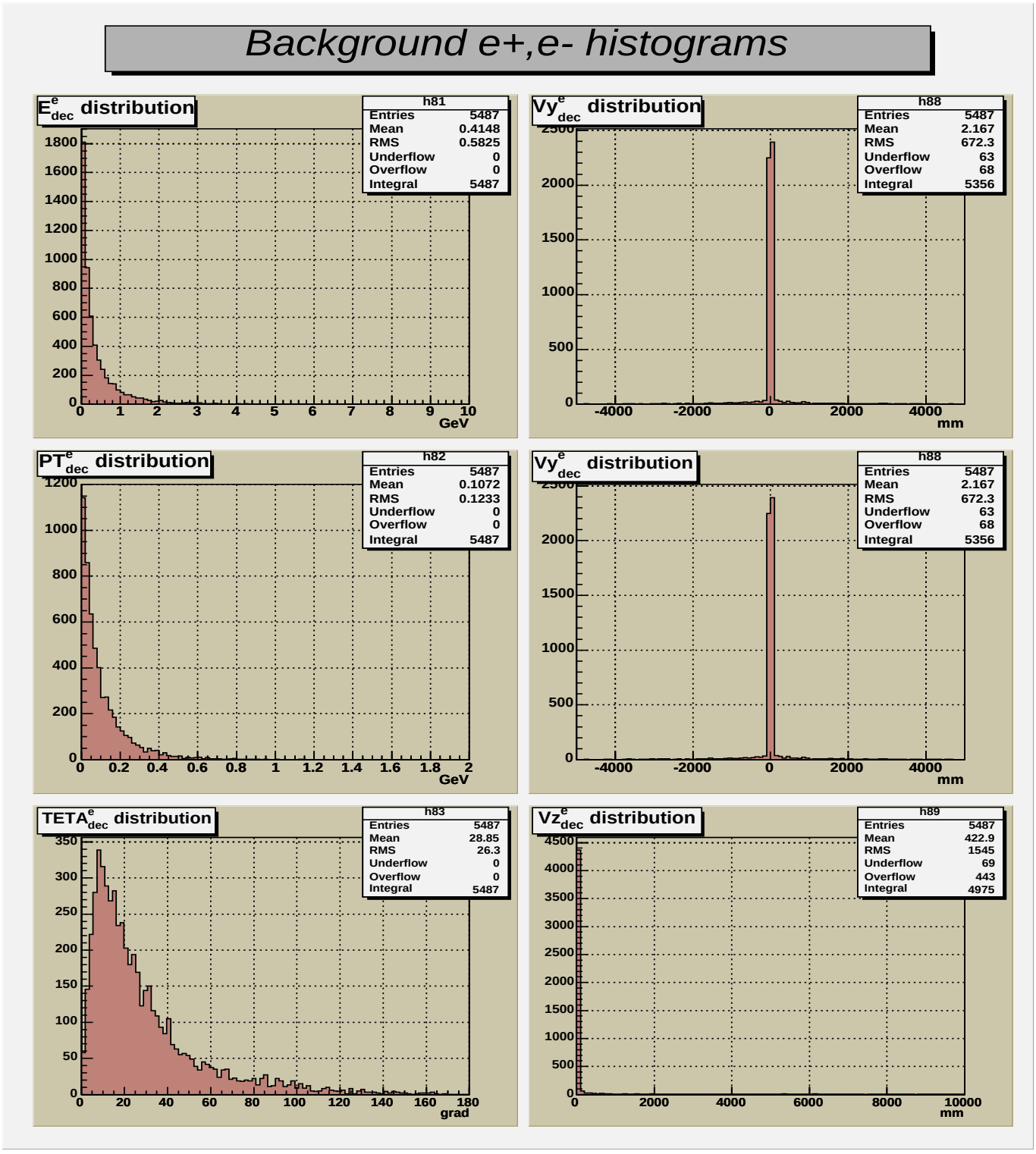

Figure 15: The left column includes the distributions (from top to bottom, respectively) of number of events versus the energy E^e_{dec}, the transverse momentum PT^e_{dec} and the polar angle θ^e_{dec} of electrons produced in QCD background events. The right column (from top to bottom) shows the distributions (in mm) of V_x-, V_y- and V_z- components of the position vector of a decay electron production vertex.